THE ASTROPHYSICAL JOURNAL SUPPLEMENT SERIES, 80:819–845, 1992 June

ZEUS-2D: A RADIATION MAGNETOHYDRODYNAMICS CODE FOR ASTROPHYSICAL FLOWS IN TWO SPACE DIMENSIONS. III. THE RADIATION HYDRODYNAMIC ALGORITHMS AND TESTS

JAMES M. STONE[1]
National Center for Supercomputing Applications, 5600 Beckman Institute, Drawer 25, 405 North Mathews Avenue, Urbana, IL 61801
DIMITRI MIHALAS
Department of Astronomy, University of Illinois at Urbana-Champaign, 1002 West Green Street, Urbana, IL 61801
AND
MICHAEL L. NORMAN[1]
National Center for Supercomputing Applications, 5600 Beckman Institute, Drawer 25, 405 North Mathews Avenue, Urbana, IL 61801
Received 1991 January 9; accepted 1991 October 29

ABSTRACT

In this, the third of a series of three papers, we conclude a detailed description of ZEUS-2D, a numerical code for the simulation of fluid dynamical flows in astrophysics including a self-consistent treatment of the effects of magnetic fields and radiation transfer. In this paper, we describe the radiation hydrodynamical (RHD) algorithms in ZEUS-2D.

We develop a two-dimensional full transport algorithm to evolve the radiation moment equations. The moment equations are closed with the tensor variable Eddington factor whose components are computed from angular quadratures of the specific intensity which, in turn, is computed from a formal solution of the two-dimensional transfer equation using the method of short characteristics. This algorithm for multidimensional RHD differs significantly from more commonly used methods based on the diffusion approximation. The results of a collection of test problems we have developed for RHD algorithms are presented.

Subject headings: hydrodynamics — methods: numerical — MHD — radiative transfer

1. INTRODUCTION

Two-dimensional radiation hydrodynamical (RHD) calculations for modeling astrophysical systems represent a frontier in theoretical astrophysics. Many physical systems have been identified in which a one-dimensional purely hydrodynamical model would be inadequate or inappropriate (for example, accretion flows onto compact objects, or radiatively driven winds from rapidly rotating or magnetic hot stars). In order to be able to model such systems, we have developed a general purpose hydrodynamics (HD) code, called ZEUS-2D, which allows for the self consistent treatment of the effects of magnetic fields and radiation transfer. In two previous papers, we have described the HD algorithms (Stone & Norman 1992a, hereafter Paper I) and the algorithms for evolving the magnetic fields (Stone & Norman 1992b, hereafter Paper II). In this paper, we describe the final major algorithm development project undertaken as part of this work: the addition of a two-dimensional radiation-transport module to ZEUS-2D. This module contains algorithms for solving the dynamical equations of the radiation field which, when coupled to the magnetohydrodynamic (MHD) algorithms described in Papers I and II, allow for the self-consistent evolution of the composite material-radiation fluid in the prescence of magnetic fields. Thus, ZEUS-2D is a radiation magnetohydrodynamics (RMHD) code.

Most multidimensional RHD calculations presented to date invoke the diffusion approximation at some level in order to simplify the calculations. In order to prevent inconsistencies in optically thin media (where the diffusion approximation is not valid), the use of an ad hoc parameter, called the "flux limiter," is generally required. However, the RHD algorithms used in ZEUS-2D, and described here, do not make use of the diffusion approximation. Instead, we close the equations of RHD by use of a tensor variable Eddington factor computed from a formal solution of the transfer equation in two-dimensions, a technique similar to that used in stellar atmosphere calculations. This full transport method is equally applicable to optically thin and thick media, and does not require the use of flux limiters.

The development of the radiation module divides naturally into two parts: (1) solving the dynamical equations of the radiation field (the moment equations) coupled to the HD for an assumed closure relation, and (2) solving the transfer equation in two-dimensions to calculate the closure. We follow this organization closely in this paper. We begin in § 2 by discussing the form of the moment equations to be used in this project, and how they are coupled to the gas dynamical equations to form the full set of equations of RMHD. In order to avoid the conceptual errors in the formulation of the equations which have plagued some work in the past, we derive the moment equations directly from the comoving transfer equation. We continue in § 3 by discussing the numerical methods developed in ZEUS-2D for solving the moment equations, while in § 4 we describe the algorithm we have implemented for solving the transfer equation, needed to close the moment equations. In § 5, we describe the changes that are

[1] Also Department of Astronomy, University of Illinois at Urbana-Champaign.

required in ZEUS-2D in order to incorporate the radiation module. In §§ 6 and 7 we present the results of the test problems we have performed on the moment and transfer equation solvers respectively, while in § 8 we summarize.

2. THE EQUATIONS OF RADIATION HYDRODYNAMICS

A radiating fluid is one in which the radiation field contains a significant fraction of the energy density, momentum density, and stress (i.e., pressure), or in which radiation is the dominant energy-exchange mechanism. In order to obtain a full description of the flow dynamics in such a fluid, the conservation laws which describe the evolution of the material quantities must be extended with conservation laws which describe the evolution of the radiation field. One can use an exactly analogous method to derive the conservation laws obeyed by the radiation field as was used to derive those for the material component of the fluid. In other words, in the same way that the gasdynamical equations are generated by taking velocity moments of the Boltzmann equation (which describes the evolution in phase space of the material particle distribution function), the radiation dynamical equations are derived by taking angular moments of the transfer equation (which describes the evolution in phase space of massless, extreme-relativistic particles called photons). Similarly, in the hierarchy of both the radiation and gas dynamical moment equations, there is a *closure problem,* requiring the elimination of the angular moment of order $n + 1$ from the first n moment equations. In gasdynamics, the moment equations are closed by an equation of state which relates the material gas pressure to the mass and energy densities. Fundamentally, the equation of state is based on the assumption that a mean free path of a particle is much smaller than any scale length in the system so that a strict local equilibrium applies, and the distribution function is very nearly isotropic. One could, in principle, close the radiation moment equations in the same way, e.g., by assuming the photon distribution function (specific intensity) is isotropic, leading to the diffusion approximation. Indeed, most RHD calculations performed to date have invoked the diffusion approximation in one form or another. However, in general, the mean free path of a photon is *not* small compared to scale lengths in the system (e.g., for optically thin regions, or near boundaries), so that the assumption of isotropy is not valid, and there is no simple closure relation for the radiation moment equations.

In this work, we attack this closure problem squarely, by actually solving the transfer equation to compute the angular distribution of the specific intensity, and then explicitly calculating the relation between two different moments (the radiation pressure and energy density), which can then be used to close the moment equations. By working to such a high degree of internal consistency, we guarantee our methods will be applicable to systems which incorporate or develop optically thin regions in the flow, situations which can lead to problems with methods based on the diffusion approximation.

In the remainder of this section, we will derive the form of the moment equations which will be used in this work, and describe how these equations are coupled to the gasdynamical equations to form a closed set of equations of RHD.

2.1. *The Comoving Moment Equations to* O(1)

Before we can develop a solution procedure for the moment equations, we must first write them down in a particular frame of reference. However, since the equations contain $O(v/c)$ frame dependent terms, this task is nontrivial. We must carefully choose a reference frame in which to solve the equations that is best suited to our problem, and then ensure that the equations contain all $O(v/c)$ terms which might arise in this frame in all physical regimes. Failure to discriminate between frames of reference, or in the consistency of the order of terms contained in the equations in a particular frame, can lead to serious errors. Note that this difficulty does not occur in gas dynamics, since the frame dependent terms for a nonradiating fluid are only $O(v^2/c^2)$ (the most familiar of which is the kinetic energy density).

In this work, we have chosen to use the comoving (or Lagrangean) frame in which each fluid parcel is instantaneously at rest. The major motivation for this choice is that, in the comoving frame, the material properties are isotropic, and thus the interaction between radiation and matter can be handled most easily. Moreover, in this frame we can describe the microphysics of the matter properly through statistical mechanical relations. This frame also corresponds closely to that used for the HD, where all dependent variables are really Lagrangean variables solved on an Eulerian mesh. Thus, in this frame one can take advantage of powerful computational tools such as adaptive meshes. However, all these advantages are countered by the fact that the equations are generally more complex in the comoving frame.

We can circumvent the complexities introduced by the comoving frame to some extent by solving the equations to $O(1)$ only. This step is completely justified for nonrelativistic flows, in which $(v/c) \ll 1$. However, it means that from the outset, the radiation module described here can only be used for nonrelativistic flows, and any other use will lead to errors.

The comoving moment equations to $O(1)$ are most easily derived from a dimensional analysis of the $O(v/c)$ equations. The latter can be derived directly from the comoving transfer equation, which in turn can be derived by two methods: (1) performing an $O(v/c)$ transformation of the inertial frame transfer equation, being careful to account for the transformation of all variables and derivatives to the comoving frame, or (2) using a direct, noninertial derivation from the photon Boltzmann equation. We do not give either derivation here but merely state the results, as the details of both methods have been described in the literature (e.g., Lindquist 1966; Castor 1972; Buchler 1979; Mihalas & Mihalas 1984; Kaneko, Morita, & Maekawa 1984; Mihalas 1988).

From these sources, we find that in the comoving frame the total (frequency integrated) zeroth and first moment equations to $O(v/c)$ can be written as

$$\rho \frac{D}{Dt}\left(\frac{E_o}{\rho}\right) + \nabla \cdot \boldsymbol{F}_o + \frac{2\boldsymbol{a} \cdot \boldsymbol{F}_o}{c^2} + \nabla \boldsymbol{v} : \mathbf{P}_o = \int_0^\infty [4\pi\eta_o(\nu_o) - c\chi_o(\nu_o)E_o(\nu_o)]d\nu_o \,, \tag{1}$$

$$\frac{\rho}{c^2}\frac{D}{Dt}\left(\frac{\boldsymbol{F}_o}{\rho}\right)+\nabla\cdot\mathbf{P}_o+\frac{1}{c^2}(\boldsymbol{a}\cdot\mathbf{P}_o+\boldsymbol{a}E_o)+\frac{1}{c^2}(\nabla\boldsymbol{v}\cdot\boldsymbol{F}_o)=-\frac{1}{c}\int_0^\infty\chi_o(\nu_o)\boldsymbol{F}_o(\nu_o)d\nu_o\,, \tag{2}$$

where the D/Dt denotes a Lagrangean derivative, E_o, $\boldsymbol{F}_o$, and $\mathbf{P}_o$ are the comoving radiation internal energy density, flux and stress tensor respectively, $\boldsymbol{a}$ is the fluid acceleration ($\boldsymbol{a}\equiv d\boldsymbol{v}/dt$), and the other symbols have their usual meaning. The subscript on the radiation variables denotes that these quantities are measured in the comoving frame. The closure problem is evident in these equations, as we have four equations in 10 unknowns (E_o, $\boldsymbol{F}_o$, and $\mathbf{P}_o$). We close the system using the tensor variable Eddington factors, as described in the next section.

Each term in equations (1) and (2) has a direct physical interpretation (Castor 1972). For instance, in equation (1) (the radiation energy equation), the terms are (in order from left to right) the rate of change of the radiation energy density, the rate of transport of radiation energy, the equivalent inertia of radiant energy flow, the rate at which radiation pressure is doing work, and the rate at which energy is being added to the radiation field due to interactions with matter (all terms are per unit volume). Similarly, in equation (2) (the radiation momentum equation), the terms are (from left to right) the rate of change of the radiation momentum density, the rate of transport of radiation momentum, the equivalent inertia of the radiation enthalpy density, the interaction of the radiation momentum density with a shear flow field, and the net rate of addition of momentum to the radiation momentum density due to interactions with matter. Equations (1) and (2) can account for all the dynamical effects of radiation on a fluid flow time scale to $O(v/c)$ (Mihalas & Mihalas 1984). In addition to their physical significance, the moment equations are also powerful tools for solving transfer problems because they eliminate angle variables from the problem and thereby reduce its dimensionality. This fact underlies the reason we choose to describe the evolution of the radiation field using the moment equations rather than solving, for example, the time-dependent transfer equation.

At this point, we wish to reduce the moment equations to $O(1)$ by dropping terms which are $O(v/c)$ *in all physical regimes*. To be self-consistent, we must ensure that any term which is $O(1)$ in any one regime is kept, even if it is formally $O(v/c)$ in some other regime. This step is of vital importance, as it is possible that terms which are formally $O(v/c)$ in some regime may actually dominate the equations in other regimes.

There are three regimes of interest to us:

1. the streaming limit ($\lambda_p/l\geq 1$), where λ_p is a photon mean free path and l is a characteristic length scale of the system, and $P\approx E$ and $F\approx cE$,
2. the static diffusion limit ($v/c\ll\lambda_p/l$), where $P\approx\frac{1}{3}E$ and F/cE is $O(\lambda_p/l)$,
3. the dynamic diffusion limit ($v/c\geq\lambda_p/l$), where $P=\frac{1}{3}E$ and F/cE is $O(v/c)$.

The first limit corresponds to radiation streaming in an optically thin fluid, the second to radiation diffusing in an essentially motionless, optically thick medium, while the third to radiation being advected in an optically thick, moving medium. In each regime, we can perform a dimensional analysis on a fluid flow time scale of the $O(v/c)$ moment equations by replacing the time derivative $\partial/\partial t$ with l/v and the spatial gradient ∇ with $1/l$. Thus, in the various limits, the terms in the radiation energy equation scale as

streaming limit	v/c	1	$(v/c)^2$	v/c	l/λ_p,
static diffusion	$(v/c)(l/\lambda_p)$	1	$(v/c)^2$	$(v/c)(l/\lambda_p)$	1,
dynamic diffusion	1	$(c/v)(\lambda_p/l)$	$(v/c)(\lambda_p/l)$	1	1.

Since any term which is $O(1)$ in any regime must be kept, we must keep the first, second, fourth and last terms in equation (1). Next, the terms in the radiation momentum equation scale as

streaming limit	v/c	1	$(v/c)^2$	$(v/c)^2$	v/c	$1/\lambda_p$,
diffusion limit	$(v/c)(\lambda_p/l)$	1	$(v/c)^2$	$(v/c)^2$	$(v/c)(\lambda_p/l)$	1.

Thus, the correct $O(1)$ equation requires keeping the first, second and last term in equation (2). We therefore conclude that the complete comoving moment equations to $O(1)$ are

$$\rho\frac{D}{Dt}\left(\frac{E_o}{\rho}\right)+\nabla\cdot\boldsymbol{F}_o+\nabla\boldsymbol{v}:\mathbf{P}_o=\int_0^\infty[4\pi\eta_o(\nu_o)-c\chi_o(\nu_o)E_o(\nu_o)]d\nu_o\,, \tag{3}$$

$$\frac{\rho}{c^2}\frac{D}{Dt}\left(\frac{\boldsymbol{F}_o}{\rho}\right)+\nabla\cdot\mathbf{P}_o=-\frac{1}{c}\int_0^\infty\chi_o(\nu_o)\boldsymbol{F}_o(\nu_o)d\nu_o\,. \tag{4}$$

These equations can account for all the dynamical effects of radiation in a nonrelativistic fluid, where $v/c\ll 1$, so that we can ignore terms of $O(v/c)$.

2.2. *Coupling the Moment Equations to the Hydrodynamics*

The radiation field can influence the material component of the fluid via (1), momentum exchange which can accelerate or decelerate the flow, and (2) energy exchange which can heat or cool the fluid. Thus, the interaction of radiation with matter is accounted for by adding terms to the momentum and energy equations, respectively. If we add the material and radiation internal energy equations, the full set of equations of RMHD to be solved is

$$\frac{D\rho}{Dt} + \rho\nabla\cdot\boldsymbol{v} = 0\,, \tag{5}$$

$$\rho\frac{D\boldsymbol{v}}{Dt} = -\nabla p - \rho\nabla\Phi + \frac{1}{4\pi}(\nabla\times\boldsymbol{B})\times\boldsymbol{B} + \frac{1}{c}\chi_F\boldsymbol{F}\,, \tag{6}$$

$$\rho\frac{D}{Dt}\left(\frac{E}{\rho}\right) = -\nabla\cdot\boldsymbol{F} - \nabla\boldsymbol{v}:\mathbf{P} + 4\pi\kappa_P B - c\kappa_E E\,, \tag{7}$$

$$\rho\frac{D}{Dt}\left(\frac{e+E}{\rho}\right) = -\nabla\boldsymbol{v}:\mathbf{P} - p\nabla\cdot\boldsymbol{v} - \nabla\cdot\boldsymbol{F}\,, \tag{8}$$

$$\frac{\rho}{c^2}\frac{D}{Dt}\left(\frac{\boldsymbol{F}}{\rho}\right) = -\nabla\cdot\mathbf{P} - \frac{1}{c}\chi_F\boldsymbol{F}\,, \tag{9}$$

$$\frac{\partial\boldsymbol{B}}{\partial t} = \nabla\times(\boldsymbol{v}\times\boldsymbol{B})\,, \tag{10}$$

$$\nabla^2\Phi = 4\pi G\rho\,, \tag{11}$$

where we have assumed LTE, so that the source function $S = \eta/\chi$ is identical to the Planck function B, and we have introduced the flux mean, Planck mean and energy mean opacities

$$\chi_F \equiv \frac{1}{F}\int_0^\infty \chi(\nu)F(\nu)d\nu\,, \tag{12}$$

$$\kappa_P \equiv \frac{1}{B}\int_0^\infty \chi(\nu)B(\nu)d\nu\,, \tag{13}$$

$$\kappa_E \equiv \frac{1}{E}\int_0^\infty \chi(\nu)E(\nu)d\nu\,. \tag{14}$$

Note that we have dropped the subscripts on all radiation variables, although we emphasize that these quantities are still measured in the comoving frame. The advantage of adding the material and radiation energy equations to form the first law of thermodynamics for the radiating fluid (eq. [8]), rather than solving each equation separately, is that the material-radiation interaction terms have cancelled on the RHS, which ensures our numerical scheme will be accurate when the fluid is near radiative equilibrium. The full set of RMHD equations are closed with constitutive relations for the material gas pressure, opacities and the Planck function, [i.e., $p = p(\rho, e)$, $\chi_F = \chi_F(\rho, e)$, $\kappa_E = \kappa_E(\rho, e)$, $\kappa_P = \kappa_P(\rho, e)$, and $B = B(\rho, e)$]. In addition, we close the radiation moment equations (7)–(9) with the tensor variable Eddington factor $\mathbf{f}$ which is used to eliminate the radiation stress tensor $\mathbf{P}$ (second angular moment) in favor of the radiation energy density E (zeroth angular moment) via

$$\mathbf{P} = \mathbf{f}E\,. \tag{15}$$

The tensor Eddington factors are computed, in turn, from numerical quadratures of the specific intensity,

$$\mathbf{f} = \frac{\mathbf{P}}{E} = \frac{\oint I\boldsymbol{n}\boldsymbol{n}d\omega}{\oint Id\omega}\,, \tag{16}$$

where the integrals are taken over solid angle, and the specific intensity $I(\boldsymbol{x}, \boldsymbol{n}, \nu)$ is calculated from a formal solution of the transfer equation

$$\frac{\partial I}{\partial s} = \chi(S - I)\,. \tag{17}$$

In the past, closing the RHD problem using the tensor variable Eddington factor computed from a formal solution of the full angle-frequency dependent transfer equation in a multidimensional numerical algorithm has been considered to be too computationally expensive; thus most previous work on two-dimensional RHD has generally made use of the nonequilibrium diffusion approximation, in which the Eddington approximation ($f_{ii} = \frac{1}{3}$, and $f_{ij} = 0$ for $i \neq j$) is used. This circumvents the need for a formal solution of the transfer equation. However, although this method results in considerable reduction of the computational demands of the problem, it is really applicable only to optically thick flows so that the radiation field is isotropic, and may not give the correct result if the radiation becomes streaming *anywhere* on the grid. Furthermore, there is no a priori way to know whether or not a particular flow will become optically thin somewhere on the grid. Applying the diffusion approximation to calculations of optically thin flows leads to the classic problem of "flux-limiting." Numerical fix-ups of this problem, such as "flux-limiters," are of unknown generality and reliability, and therefore may not always be satisfactory. Only a full transport solution can treat correctly the kinds of situations we expect to occur in many astrophysical systems, such as direct irradiation of a local optically thin region (for example, the envelope of an accretion disk) by a remote source of intense radiation (the central object).

For these reasons, we have implemented algorithms for solving the coupled radiation moment equations (7)–(9), and for solving the transfer equation (17) in two dimensions (to compute the Eddington factors from eq. [16]). However, in order to make the problem tractable, we proceed by solving the moment equations independently of the transfer equation, assuming the Eddington factors are already known. Once this step is completed, the Eddington factors are updated using the new physical structure of the fluid. Of course, in general the Eddington factors are not strictly independent of the solution of the moment equations, and therefore ideally one should solve the moment and transfer equations concurrently. The most efficient method of achieving this is to iterate between successive solutions of the moment and transfer equations until consistency between the results is achieved. However, in multidimensional HD calculations, it is still not feasible to work to such a high degree of self-consistency. This is because the solution of the radiation moment equations can take as much as 10 times the cpu time as all of the rest of the HD algorithms combined (for an explicit code), so that one cannot afford to solve the moment equations more than once per time step. Therefore, one must use independent solutions of the moment and transfer equations, without iterating to consistency. This procedure works because the Eddington factor is a measure of the anisotropy of the radiation field. In most circumstances the geometry of the field and therefore the Eddington factors will not change much over one (or more) time steps. Therefore, lagging the Eddington factors by one (or more) time steps will generally not introduce serious errors. This is not the case, however, when the system evolves on a radiation flow time scale (such as when an ionization front penetrates a cold medium, or emerges from a hot dense material into near vacuum). In such circumstances, one cannot split the solutions of the moment and transfer equations, and an iterative technique is essential. Nevertheless, by closing the moment equations with the Eddington factors computed from a formal solution of the transfer equation rather than with arbitrary flux limiters, the full transport algorithm in ZEUS-2D for RHD is a considerable improvement over flux-limited diffusion schemes.

Finally, it is useful to examine the assumptions and restrictions that we have built into the RMHD equations as written. Firstly, we have kept only terms to $O(1)$ in the radiation moment equations, so that we cannot apply this system of equations to relativistic flows. This is consistent with the MHD equations, which are also nonrelativistic. Secondly, we have assumed LTE, so that the source function in equation (7) is identical to the Planck function. Relaxing the LTE assumption requires solving a delicate system of rate equations which describes the thermodynamic state of the material component of the fluid. However, given that solving the coupled radiation moment-rate equations is already a formidable task, requiring an iterative method (as is used, for example, in stellar atmosphere calculations), it seems clear that using current techniques multidimensional non–LTE RHD simulations will require substantially more computing resources than is currently available. (Such is not the case in one dimension, where Klein et al. (1988) have developed a method to treat the non-LTE frequency dependent radiation transfer problem coupled to hydrodynamics.) Finally, we have also suppressed the frequency dependence of radiation transfer by using only total (frequency integrated) variables and mean opacities in the transfer equation. In static problems, and one-dimensional HD, frequency dependent transfer is practical, and numerical methods for such problems are well developed (e.g., multigroup methods). It may be profitable to consider frequency dependent transport in future work, both in the dynamics and to post-process flow fields by computing maps of the emergent intensity.

3. SOLVING THE MOMENT EQUATIONS

In the operator split formalism used to evolve the HD, the evolution equations are updated in two independent steps, the source and the transport steps (see Paper I). We can use this formalism to update the radiation moment equations by expanding the Lagrangean derivatives with the continuity equation to separate the source and advection terms. Then, in the source step, we solve finite difference approximations to

$$\frac{\partial E}{\partial t} = -\nabla \cdot \boldsymbol{F} - \nabla \boldsymbol{v} : \mathbf{P} + 4\pi \kappa_P B - c\kappa_E E \,, \tag{18}$$

$$\frac{\partial (e + E)}{\partial t} = -\nabla \boldsymbol{v} : \mathbf{P} - p \nabla \cdot \boldsymbol{v} - \nabla \cdot \boldsymbol{F} \,, \tag{19}$$

$$\frac{1}{c^2} \frac{\partial \boldsymbol{F}}{\partial t} = -\nabla \cdot \boldsymbol{P} - \frac{1}{c} \chi_F \boldsymbol{F} \,, \tag{20}$$

while in the transport step, we use an integral formulation to develop a conservative differencing scheme for

$$\frac{d}{dt}\int_V E dV = -\oint_{dV} E(\boldsymbol{v} - \boldsymbol{v}_g)\cdot d\boldsymbol{S}\,, \tag{21}$$

$$\frac{d}{dt}\int_V (e+E) dV = -\oint_{dV} (e+E)(\boldsymbol{v} - \boldsymbol{v}_g)\cdot d\boldsymbol{S}\,, \tag{22}$$

$$\frac{d}{dt}\int_V \boldsymbol{F} dV = -\oint_{dV} \boldsymbol{F}(\boldsymbol{v} - \boldsymbol{v}_g)\cdot d\boldsymbol{S}\,, \tag{23}$$

where $\boldsymbol{v}_g$ is a grid velocity to account for grid motion. Note, however, that since $\boldsymbol{F}$ is a vector quantity, using the scalar divergence theorem to write the advection terms in the form of equation (23) will again lead to terms in non-Cartesian geometry which arise due to the divergence operator acting on unit vectors (as it did for the equation of motion, see Paper I).

Mathematically, the radiation moment equations are a set of coupled advection-diffusion equations. To demonstrate this, we can write the radiation energy equation in both the streaming limit (where $F \approx cE$), and the static diffusion limit [where $F \approx -(c/3\chi)\nabla E$] assuming a static medium in radiative equilibrium. Thus,

$$\text{streaming limit} \qquad \partial E/\partial t = -\nabla\cdot cE\,,$$

$$\text{diffusion limit} \qquad \partial E/\partial t = \nabla\cdot(c/3\chi)\nabla E\,.$$

Clearly, in the streaming limit, the radiation energy equation is an advection equation with the characteristic speed being the speed of light c. In the static diffusion limit, it is a diffusion equation, with an effective diffusion constant of $D \approx c/3\chi$. If we were to solve the radiation moment equations with a time explicit method, then the CFL stability criterion would include time step limits set by the characteristic speed c and an effective viscosity coefficient $\nu = D \approx c/3\chi$ (see Paper I). Clearly, these time step limits would be much more restrictive than those set by the HD. Since we are generally interested in evolving systems on dynamical time scales, rather than light crossing time scales, it is clear that although the HD can be integrated explicitly in time, the solution of the radiation moment equations *must* be implicit.

In two dimensions, assuming the Eddington tensor is given, the radiation moment equations (18)–(20) represent four equations in four unknowns, e, E, and the two nonzero components of $\boldsymbol{F}$. Solving this system implicitly represents a considerable computational challenge. We can, however, reduce the number of equations (and thereby greatly simplify the problem) by using the idea of "automatic flux limiting" (AFL) (Mihalas & Weaver 1982). Here, the radiation momentum equation (20) is integrated in time analytically, albeit in an approximate way. We can rewrite equation (20) as

$$\frac{\partial \boldsymbol{F}}{\partial t} + c\chi_F \boldsymbol{F} = -c^2\nabla\cdot(\mathbf{f}E)\,. \tag{24}$$

The integrating factor for this equation is $e^{c\chi_F t}$, thus integrating over a fluid flow time step gives

$$\boldsymbol{F}(t+\Delta t)e^{c\chi_F(t+\Delta t)} - \boldsymbol{F}(t)e^{c\chi_F t} = -c^2\int_t^{t+\Delta t} \nabla\cdot(\mathbf{f}E)e^{c\chi_F t} dt\,. \tag{25}$$

If we now choose some approximate, "average" value over the time step Δt for χ_F and $\nabla\cdot(\mathbf{f}E)$ on the RHS, then equation (25) becomes

$$\boldsymbol{F}(t+\Delta t) = e^{-x}\boldsymbol{F}(t) - (1-e^{-x})\frac{c}{\langle\chi_F\rangle}\overline{[\nabla\cdot(\mathbf{f}E)]}\,, \tag{26}$$

where $x \equiv c\langle\chi_F\rangle\Delta t$. Equation (26) represents an exponentially attenuated, stable prescription for evaluating the flux; it can handle the numerical stiffness that arises when x = (photon free flight distance in Δt/photon mean free path) $\gg 1$. The accuracy of the method will depend on how well the time-averaged values $\langle\chi_F\rangle$ and $\langle\nabla\cdot(\mathbf{f}E)\rangle$ can be approximated. In this work, we will use variable time centering, i.e., for the time-averaged value $\langle X\rangle$ we take $\langle X\rangle = X^{n+\alpha} = \alpha X^{n+1} + (1-\alpha)X^n$, where α is arbitrary, but must be larger than 0.5 for stability. Equation (26) can now be inserted algebraically into equations (18) and (19), yielding only two coupled, implicit equations for the two variables e and E. Note, however, that these equations will be highly nonlinear due to the temperature dependence of the opacities and the Planck function. Nonetheless, numerical methods for solving these equations in two-dimensions are readily available, as discussed in § 3.2.

3.1. *Centering of Variables*

Before finite-differencing the moment equations, we must first decide on a centering of the radiation variables on the staggered mesh. In general, scalars and the diagonal components of tensors of even rank are zone centered, the off-diagonal components of tensors of even rank are centered at zone corners, while tensors of odd rank are face centered. (The two-dimensional staggered mesh used in the ZEUS-2D code is described in § 4.1 of Paper I; we merely note here the mesh is labeled by the coordinate vectors x_1 and x_2, with the 3-direction taken to be orthogonal to the computational plane.) Thus, the natural centering for the primary radiation variables is (see Fig. 1)

$$E(x_1, x_2) \rightarrow E(x1b_i, x2b_j) = E_{i,j} ,$$

$$F_1(x_1, x_2) \rightarrow F1(x1a_i, x2b_j) = F1_{i,j} ,$$

$$F_2(x_1, x_2) \rightarrow F2(x1b_i, x2a_j) = F2_{i,j} ,$$

$$P_{11}(x_1, x_2) \rightarrow P11(x1b_i, x2b_j) = P11_{i,j} ,$$

$$P_{22}(x_1, x_2) \rightarrow P22(x1b_i, x2b_j) = P22_{i,j} ,$$

$$P_{33}(x_1, x_2) \rightarrow P33(x1b_i, x2b_j) = P33_{i,j} ,$$

$$P_{12}(x_1, x_2) \rightarrow P12(x1a_i, x2a_j) = P12_{i,j} .$$

The components of the tensor variable Eddington factor are centered identically to the components of the radiation stress tensor. The mean opacities and Planck function, which are derived from the zone centered mass and energy densities, are either zone centered (κ_E, κ_P, and B), or face centered (χ_F), see Figure 1. We use an energy weighted harmonic mean to compute the opacities at zone interfaces, which, since we do not use an adaptive mesh, is necessary to get reasonable energy transport at unresolved interfaces (Mihalas & Mihalas 1984). Finally, the velocity gradient is a rank-two tensor, and therefore its components are centered identically to those of the radiation stress tensor **P**. The velocity gradient tensor is also encountered in the formulation of the tensor artificial viscosity (see Paper I).

3.2. *The Source Terms*

In the source step, we solve the finite difference approximations to equations (18) and (19). We begin by discretizing in time, so

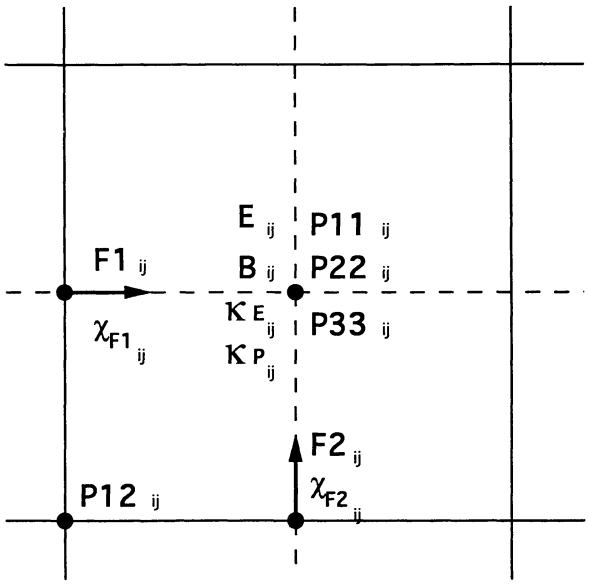

FIG. 1.—Centering of the RHD variables in the ZEUS-2D code. The radiation energy density (E) and diagonal components of the radiation stress tensor (P_{11}, P_{22}, and P_{33}) are zone centered, the components of the flux (F_1 and F_2) are face centered, and the off-diagonal component of the stress tensor (P_{12}) is located at zone corners. The centering of the Planck function (B), energy, Planck, and flux mean opacities (κ_E, κ_B, and χ_F, respectively) is also shown.

that

$$(E^{n+1} - E^n)/\Delta t = 4\pi\kappa_P^{n+\theta} B^{n+\theta} - c\kappa_E^{n+\theta} E^{n+\theta} - \nabla \cdot \boldsymbol{F}^{n+\theta} - \nabla \boldsymbol{v} : \mathbf{P}^{n+\theta} , \tag{27}$$

$$(e^{n+1} + E^{n+1} - e^n - E^n)/\Delta t = -\nabla \cdot \boldsymbol{F}^{n+\theta} - \nabla \boldsymbol{v} : \mathbf{P}^{n+\theta} - p^{n+\theta} \nabla \cdot \boldsymbol{v} , \tag{28}$$

where we have time centered each variable on the RHS, so that $X^{n+\theta} = \theta X^{n+1} + (1 - \theta) X^n$. The parameter θ is arbitrary, but must be greater than 0.5 for stability (Richtmyer & Morton 1957). Note that $\boldsymbol{F}^{n+\theta} = \theta \boldsymbol{F}^{n+1} + (1 - \theta)\boldsymbol{F}^n$, where $\boldsymbol{F}^{n+1}$ is given by the AFL formula (eq. [26]). We then discretize equations (27) and (28) in space on the staggered mesh, using the variable centering described above, so that

$$E_{i,j}^{n+1} - E_{i,j}^n - \Delta t[4\pi\kappa_{P;i,j}^{n+\theta} B_{i,j}^{n+\theta} - c\kappa_{E;i,j}^{n+\theta} E_{i,j}^{n+\theta} - (\nabla \cdot \boldsymbol{F}^{n+\theta})_{i,j} - (\nabla \boldsymbol{v} : \mathbf{P}^{n+\theta})_{i,j}] = 0 , \tag{29}$$

$$e_{i,j}^{n+1} + E_{i,j}^{n+1} - e_{i,j}^n - E_{i,j}^n - \Delta t[-(\nabla \cdot \boldsymbol{F}^{n+\theta})_{i,j} + (\nabla \boldsymbol{v} : \mathbf{P}^{n+\theta})_{i,j} - p_{i,j}^{n+\theta} (\nabla \cdot \boldsymbol{v})_{i,j}] = 0 . \tag{30}$$

Explicit finite difference equations for $(\nabla \cdot \boldsymbol{F}^{n+\theta})_{i,j}$ and $(\nabla \boldsymbol{v} : \mathbf{P}^{n+\theta})_{i,j}$ are given in Appendix A, while an expression for $(\nabla \cdot \boldsymbol{v})_{i,j}$ is given in Appendix C of Paper I. An important point is that each of the terms in equations (29) and (30) must be zone centered. On a staggered grid in two dimensions, and with use of the AFL formula, the divergence of the flux term will therefore result in a nine point difference molecule for the radiation energy density. Averaging the opacity to zone interfaces in two dimensions results in a five-point difference molecule for the material energy density (see, e.g., the difference equations in Appendix A). This has important consequences for the numerical solution of these equations.

The finite difference equations (29) and (30) are very nonlinear due to the dependence of the opacities and Planck function on e and E. In order to generate numerical solutions, the equations must be linearized, and an iterative technique used to develop the full solution. In this work, we have used the Newton-Raphson (NR) method due to its simplicity, robustness, and speed (quadratic convergence). For a system of i coupled equations in j variables which can be written as

$$\boldsymbol{f}(\boldsymbol{x}) = 0 , \tag{31}$$

the Newton-Raphson method involves choosing an initial guess to the solution $\boldsymbol{x}^\nu$ (usually the solution at the last time step) and then solving the system

$$\mathbf{J}(\boldsymbol{x}^\nu)(\delta \boldsymbol{x}^\nu) = -\boldsymbol{f}(\boldsymbol{x}^\nu) , \tag{32}$$

where $\mathbf{J}(\boldsymbol{x}^\nu)$ is the Jacobian $[\partial f_i(\boldsymbol{x}^\nu)/\partial x_j]$. Once the correction to the solution $\delta \boldsymbol{x}^\nu$ has been computed, the initial guess is updated

$$\boldsymbol{x}^{\nu+1} = \boldsymbol{x}^\nu + \delta \boldsymbol{x}^\nu , \tag{33}$$

and the system is iterated to consistency (i.e., until $\delta \boldsymbol{x}^\nu < \epsilon$, where ϵ is some convergence criterion). For the moment equations in two dimensions, we have $2N^2$ coupled equations (where N is a measure of the size of the grid on each side), each of which is a function of nine radiation energy densities and five material energy densities. Equation (32) then becomes a large, sparse-banded matrix system. Schematically, the full moment equation matrix system can be written as

$$\mathbf{a}1_{i,j}\boldsymbol{x}_{i-1,j+1} + \mathbf{a}2_{i,j}\boldsymbol{x}_{i,j+1} + \mathbf{a}3_{i,j}\boldsymbol{x}_{i+1,j+1} + \mathbf{a}4_{i,j}\boldsymbol{x}_{i-1,j} + \mathbf{a}5_{i,j}\boldsymbol{x}_{i,j} + \mathbf{a}6_{i,j}\boldsymbol{x}_{i+1,j} + \mathbf{a}7_{i,j}\boldsymbol{x}_{i-1,j-1} + \mathbf{a}8_{i,j}\boldsymbol{x}_{i,j-1} + \mathbf{a}9_{i,j}\boldsymbol{x}_{i+1,j-1} = \boldsymbol{S}_{i,j} , \tag{34}$$

where $\boldsymbol{x}_{i,j} = (e_{i,j}, E_{i,j})$, $\boldsymbol{S}_{i,j}$ represents the RHS of equation (32), and the coefficients $\mathbf{a}1_{i,j}, \ldots, \mathbf{a}9_{i,j}$ result from the Jacobian derivatives. Since there are two moment equations in two unknowns, the coefficients will be 2×2 blocks. Figure 2 gives a schematic diagram of the banded pattern of the full radiation moment equation matrix.

One salient feature of implicit methods is that the boundary conditions for the dependent variables must be incorporated directly into the matrix elements themselves. For Neumann boundary conditions (for which $\partial f/\partial x = 0$), the elements on the diagonal which represent the coefficients of $e_{i,j}$ and $E_{i,j}$ for the (i, j)th equations are modified by the boundary conditions, whereas for Dirichlet boundary conditions (for which a value for f is specified), the RHS of the system is modified. We have implemented the same five boundary conditions for the radiation variables as is described in Paper I for the HD variables. Thus, we note that the reflecting, axis of symmetry, and outflow boundary conditions are all Neumann, while the inflow boundary condition is Dirichlet.

Generating expressions for the Jacobian of the moment equations, properly accounting for boundary conditions, is a tedious and time consuming task. With the nine and five point difference molecules for E and e, respectively, the Jacobian involves fourteen derivatives for each difference equation (29) and (30) (one for each dependent variable). The calculation of the Jacobian, involving taking derivatives of the finite difference equations (29) and (30) for all 14 dependent variables will not be discussed in detail here, but details can be provided on request. The derivatives are then assembled into the sparse matrix, and when combined with the RHS and an initial guess for the solution, the system can be fed into a sparse linear system solver to generate a solution.

Numerical methods to solve the type of matrix generated by the radiation moment equations are widely available. In this work,

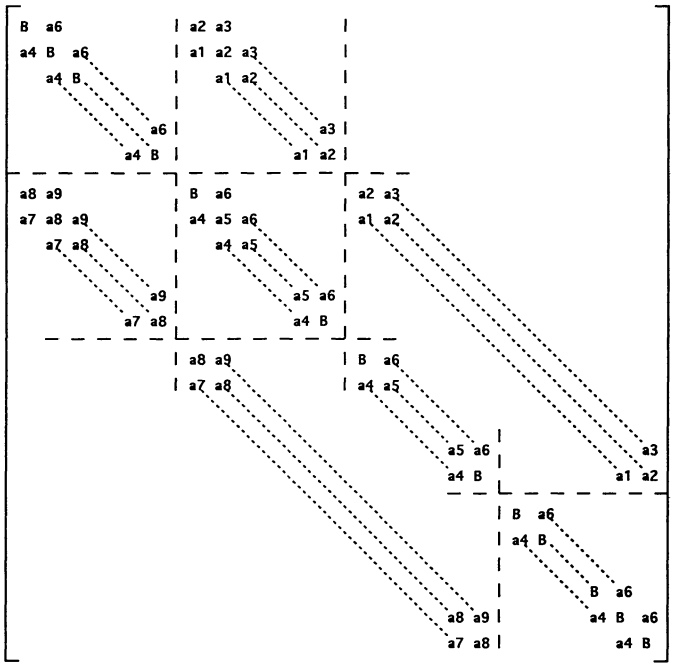

FIG. 2.—Schematic structure of the sparse banded matrix resulting from the implicit solution of the linearized radiation moment equations in two dimensions. The **a**1, . . . , **a**9 are 2×2 blocks which represent the coefficients of the two dependent variables (e and E) in the full matrix eq. (34). A value of **B** indicates that each element of the block may be affected by Neumann boundary conditions.

we have implemented a form of the general mean residual (GMRES) algorithm (Bramley 1989). Although this algorithm is very robust and efficient, it nonetheless has poor convergence properties when the Courant number becomes very large (i.e., when the HD time scale on which the equations are evolved becomes much greater than the CFL stability criterion required if the system were to be evolved explicitly). For this reason, we have begun to implement and test new and more efficient sparse solvers into the radiation molecule. Because the majority of cpu time required for the radiation module is spent in solving the sparse system (and in general, more than one sparse system must be solved at every time step due to the NR iteration), improving the performance of the solvers is very important.

The convergence of the nonlinear system is controlled by a solution procedure similar to that used in the WH80s code (Winkler & Norman 1986). Major features of the control procedure are that successive iterations of the NR method are never allowed to modify the solution by more than $\sim 10\%$, while the overall change to a variable produced by all iterations is never allowed to be more than $\sim 10\%$. Convergence is defined when successive iterations do not change the solution by more than ϵ, where $\epsilon \sim 10^{-5}$. Typically, we find that the Newton-Raphson method will converge in 4–8 steps. If the solution has not converged to within ϵ after 20 steps, the time step is reduced and the entire iteration procedure is restarted. If a time step reduction is required, the moment equations are evolved at this reduced time step until one full HD time step is completed, at which point control is returned to the HD equations. If more than six time step reductions are required, we say the solution has diverged and the computation is terminated.

3.3. *The Transport Terms*

Once the implicit update of the coupled moment equations is completed, the radiation variables must still be evolved using the advection terms. This process, however, does not need to be implicit. Indeed, the advection of the radiation variable proceeds exactly as that for the other HD variables, as described in Paper I, subject to the same time step constraint. Having expressed the advection terms in integral form in equations (21)–(23), we apply the same conservative differencing scheme as is used for the HD variables. Thus, we compute the flux of each quantity across every zone interface using one of the interpolation algorithms described previously (either donor cell, van Leer or PPA), and then use these fluxes to update the variables in a directionally split fashion.

Following the advection algorithms for the HD, we can therefore immediately generate the difference formula for the radiation variables. Thus, fluxes of each variable in the 1-direction are constructed using

$$\mathscr{F}^1_{i,j} = (E/d)^*_{1,i,j} \dot{M}^1_{i,j} g2a_i^{n+1/2} g31a_i^{n+1/2} dvl2a_j^n , \tag{35}$$

$$\mathscr{G}^1_{i,j} = (F1/d)^*_{1,i,j} \tfrac{1}{2}(\dot{M}^1_{i,j} + \dot{M}^1_{i+1,j}) g2b_i^{n+1/2} g31b_i^{n+1/2} dvl2a_j^n , \tag{36}$$

$$\mathscr{H}^1_{i,j} = (F2/d)^*_{1,i,j} \tfrac{1}{2}(\dot{M}^1_{i,j} + \dot{M}^1_{i,j-1}) g2a_i^{n+1/2} g31a_i^{n+1/2} dvl2b_j^n , \tag{37}$$

where the mass fluxes in the 1-direction $\dot{M}^1_{i,j}$ are defined by equation (55) in Paper I. These fluxes are used to update the variables due to advection in the 1-direction via

$$(E^{n+1}_{i,j}dvl1a^{n+1}_i dvl2a^n_j - E^n_{i,j}dvl1a^n_i dvl2a^n_j)/\Delta t = -(\mathscr{F}^1_{i+1,j} - \mathscr{F}^1_{i,j}) , \tag{38}$$

$$(F1^{n+1}_{i,j}dvl1b^{n+1}_i dvl2a^n_j - F1^n_{i,j}dvl1b^n_i dvl2a^n_j)/\Delta t = -(\mathscr{G}^1_{i,j} - \mathscr{G}^1_{i-1,j}) , \tag{39}$$

$$(F2^{n+1}_{i,j}dvl1a^{n+1}_i dvl2b^n_j - F2^n_{i,j}dvl1a^n_i dvl2b^n_j)/\Delta t = -(\mathscr{H}^1_{i+1,j} - \mathscr{H}^1_{i,j}) . \tag{40}$$

As soon as the advection in the 1-direction is complete, fluxes in the 2-direction are computed using

$$\mathscr{F}^2_{i,j} = (E/d)^*_{2,i,j}\dot{M}^2_{i,j}g31b^n_i dx1b^n_i g32a^{n+1/2}_j , \tag{41}$$

$$\mathscr{G}^1_{i,j} = (F1/d)^*_{2,i,j}\tfrac{1}{2}(\dot{M}^2_{i,j} + \dot{M}^2_{i-1,j})g31a^n_i dx1b^n_i g32a^{n+1/2}_j , \tag{42}$$

$$\mathscr{H}^2_{i,j} = (F2/d)^*_{2,i,j}\tfrac{1}{2}(\dot{M}^2_{i,j} + \dot{M}^2_{i,j+1})g31b^n_i dx1a^n_i g32b^{n+1/2}_j , \tag{43}$$

where the mass fluxes in the 2-direction $\dot{M}^2_{i,j}$ are defined by equation (56) in Paper I. These fluxes are then used to update the variables due to advection in the 2-direction via

$$(E^{n+1}_{i,j}dvl1a^n_i dvl2a^{n+1}_j - E^n_{i,j}dvl1a^n_i dvl2a^n_j)/\Delta t = -(\mathscr{F}^2_{i,j+1} - \mathscr{F}^2_{i,j}) , \tag{44}$$

$$(F1^{n+1}_{i,j}dvl1b^n_i dvl2a^{n+1}_j - F1^n_{i,j}dvl1b^n_i dvl2a^n_j)/\Delta t = -(\mathscr{G}^2_{i,j+1} - \mathscr{G}^2_{i,j}) , \tag{45}$$

$$(F2^{n+1}_{i,j}dvl1a^n_i dvl2b^{n+1}_j - F2^n_{i,j}dvl1a^n_i dvl2b^n_j)/\Delta t = -(\mathscr{H}^2_{i,j} - \mathscr{H}^2_{i,j-1}) . \tag{46}$$

Note that in order to reduce the relative diffusion of the radiation variables due to truncation errors, we have used the consistent advection algorithm, so that quantities are advected consistent with the mass fluxes.

Finally, as stated previously, the scalar divergence theorem used in writing the advection terms for the flux does not account for all the terms in the covariant form of the radiation momentum equation in a curvilinear coordinate system. Thus, we add the following "source terms" to the momentum equation

$$(F1^{n+1}_{i,j} - F1^n_{i,j})/\Delta t = \frac{\langle v2\rangle_{i,j}\langle F2\rangle_{i,j}}{g2a_i}\left(\frac{\partial g2a_i}{\partial x_1}\right), \tag{47}$$

$$(F2^{n+1}_{i,j} - F2^n_{i,j})/\Delta t = \frac{v2_{i,j}\tfrac{1}{4}(F1_{i,j} + F1_{i+1,j} + F1_{i,j-1} + F1_{i+1,j-1})}{g2b_i}\left(\frac{\partial g2b_i}{\partial x_1}\right), \tag{48}$$

$$\langle v2\rangle_{i,j} = (v2_{i-1,j+1} + v2_{i,j+1} + v2_{i-1,j} + v2_{i,j})/4 , \tag{49}$$

$$\langle F2\rangle_{i,j} = (F2_{i-1,j+1} + F2_{i,j+1} + F2_{i-1,j} + F2_{i,j})/4 . \tag{50}$$

4. SOLVING THE TRANSFER EQUATION

In order to close the hierarchy of radiation moment equations with the tensor variable Eddington factor, the angular distribution of the radiation field must be computed from a formal solution of the transfer equation. In this work, we assume that this step can be split from the implicit solution of the coupled moment equations (described in § 3.2). Moreover, we assume LTE, so that the source function and opacities are functions only of the local material properties. Consistent with these approximations, in this section we need only consider solving the static transfer equation, since time-dependent terms will be important only when the system evolves on a radiation flow time scale (a situation in which our assumptions will fail). In other words, we consider the fluid to be frozen in a particular state, and we solve the transfer equation to compute the radiation field propagating through the fluid at that instant.

Even assuming a static medium, solving the transfer equation is difficult due to the high dimensionality of the problem. At every four-dimensional point in space-time, the frequency independent specific intensity is a function of two angles which specify a direction of propagation (see Fig. 3). Thus, even assuming axisymmetry and a static medium, the specific intensity is four-dimensional. In order to generate a finite difference approximation to the transfer equation in two dimensions, we must discretize the four-dimensional space-angle domain. Moreover, accurately resolving the radiation field in angle is vital, since it is precisely this angular variation that determines the Eddington factors.

Currently, the most efficient transfer equation solvers exploit the symmetry and properties of the coordinate system being used, therefore it is very difficult to develop a covariant transfer equation solver with these methods (covariant forms for the transfer equation are given by, e.g., Kaneko et al. 1984 and Munier & Weaver 1984). This is not the case for the rest of the dynamical

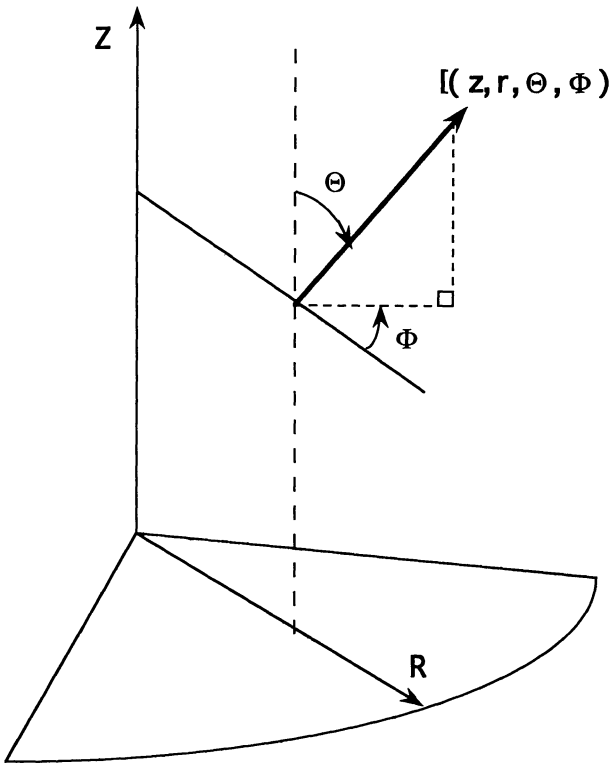

FIG. 3.—In two-dimensional cylindrical geometry, the time and frequency independent specific intensity is four-dimensional. It is a function of the two spatial coordinates Z and R, and the angles that the direction of propagation make with the Z and R axes, Θ and Φ, respectively.

equations, where developing a covariant formalism merely requires differencing the covariant forms for the vector and tensor operators in the equations. Thus, in what follows, we restrict ourselves to cylindrical and Cartesian geometry only.

4.1. *The Radiation Grid*

The first step in generating a numerical solution to the transfer equation is to develop a discrete grid on which it can be differenced. The grid used for the HD is not sufficient as it only resolves the spatial coordinates of the specific intensity; we must still discretize in angle. Since in a flat (Minkowski) spacetime, the paths of photons (geodesics) are straight lines, it is natural to consider differencing the transfer equation along these rays. At a given point in space, a discrete set of rays, each at a different angle Θ to the axis of symmetry, can be used to resolve the radiation field in polar angle Θ. This collection of rays will form a plane parallel to the axis of symmetry. In order for the radiation field to be known at every spatial position on the HD grid, we must use many planes, each tangent to a different radial shell formed by the HD grid (see Fig. 4). Each tangent plane is labeled by an impact parameter, which is just the radial coordinate of the intersected shell. If there are N radial grid points, then N tangent planes will be needed. From Figure 4, it is evident that each tangent plane intersects many radial shells, and that the azimuthal angle Φ that the outward radial unit vector makes with the tangent plane is different at each intersection. Thus, for a given radial shell, the full azimuthal description of the radiation field can be obtained by assimilating information from the intersections of this shell with many different tangent planes. To resolve the azimuthal variation of the radiation field on the first radial shell (first radial grid zone), we need an additional set of C core tangent planes which pierce this first shell. The number of intersections of a radial shell with tangent planes increases as the shell radius increases, implying that the radiation field is better resolved in azimuthal angle at large radial distances. In general, however, this is a beneficial situation because we expect the radiation field to be nearly isotropic in the core and to become strongly peaked at large radii.

On each plane, the spatial mesh on which the transfer equation is solved (which we call the radiation grid), is determined by a geometric projection of the HD mesh (see Fig. 4). The horizontal coordinate of the radiation grid is labeled x, with zones ranging from $ix = 1, nx$; the vertical coordinate is labeled z, with zones ranging from $iz = 1, nz$. The number of zones in the horizontal coordinate, nx, is determined by the impact parameter of the plane and the number of radial meshpoints on the HD grid (outside the core, nx is a steadily decreasing function of the impact parameter). The number of zones in the vertical direction, nz, is given directly from the number of axial mesh points on the HD grid, and whether or not the problem has equatorial symmetry. In order to resolve fully the radiation field in polar angle Θ at all points in space, the radiation grid must span the full domain $-Z \le z \le +Z$, even if the problem possesses equatorial symmetry (see § 4.3). We note that although the grid induced by intersections of tangent planes with radial shells is rectangular, the zone spacing in the x-direction is not equal even if the HD grid spacing is equidistant.

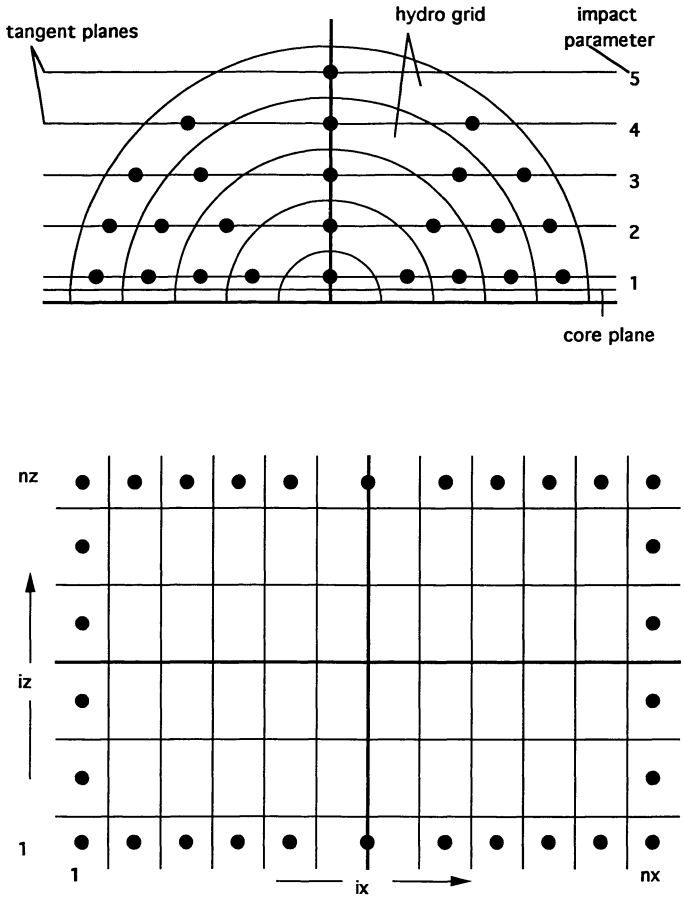

FIG. 4.—(*top*) View down the axis of symmetry of the cylindrical HD grid projected into three dimensions shows the intersection of various tangent planes on which the transfer equation is solved with radial shells defined by the two-dimensional HD grid. The semicircular lines denote the *a*-grid of the HD mesh. The tangent planes (labeled by impact parameter) are tangent to each *b*-grid shell. The dots label the points where the tangent planes and the HD *b*-grid intersect, and therefore mark the locations where the specific intensity is centered. (*bottom*) View of the radiation grid on the tangent plane numbered 1 above. The radiation grid zones are defined by the projection of the HD mesh. The axial coordinate Z is vertical in this figure, the radial coordinate R is horizontal; the axis of symmetry is shown as a bold vertical line. Boundary conditions for the specific intensity must be supplied for all dotted points.

The material properties needed to compute the opacities and source function are also given by geometric projections from the HD mesh. Boundary conditions for the specific intensity are applied along the lower and left sides of the radiation grid for $0 \leq \Theta \leq \pi/2$, and along the left and upper sides for $\pi/2 \leq \Theta \leq \pi$.

We therefore see that the radiation field is resolved in space by solving the transfer equation on many different planes, each tangent to a radial shell. The field is resolved in polar angle Θ by using many different rays on each plane. Finally, the field is then automatically resolved in azimuthal angle Φ by an astute geometrical trick, which assimilates the azimuthal variation on each radial shell from the intersections of that shell with many different tangent planes. Computing the four-dimensional specific intensity is therefore achieved by solving the transfer equation at N^2 spatial grid points on the HD mesh, using $N + C$ tangent planes, with M polar angles on each plane.

While the geometrical trick used to reduce the azimuthal angle makes the problem simpler by providing an efficient way of synthesizing the full angular variation of the radiation field, it also has some disadvantages. It is precisely this geometrical trick that makes developing a covariant transfer equation solver very difficult. We have directly used the cylindrical geometry of the problem to choose the impact parameters for the tangent rays. Moreover, we have used the azimuthal symmetry of the HD mesh to assimilate the azimuthal angle variation of the radiation field by treating each point on a given shell as equivalent. This trick will not work for three-dimensional HD grids, and is more difficult to implement in other axisymmetric coordinate systems (e.g., spherical polar). Moreover, one has no freedom in the choice of discrete values of Φ, they are given directly from the intersections of tangent planes and radial shells. Thus, there is no possibility of implementing an adaptive algorithm with which to discretize in azimuthal angle. Furthermore, since the discrete values are given by $\Phi \sim \arccos(\Delta r/r)$, for the innermost radial shells it is not possible to resolve the radiation field at small Φ (since near the axis of symmetry $r \sim \Delta r$).

In order to circumvent these problems, one cannot use the method of generating the radiation grid described here for other geometries. A fully covariant transfer equation solver could in principle be developed based on the covariant form of the transfer equation, which includes both spatial and angular derivatives (we have avoided the latter here by solving the transfer equation along

straight rays which represent geodesics). In this case, the spatial and angular coordinates could be treated as independent, and it may be possible to implement an adaptive mesh algorithm to resolve the angular variation of the radiation. However, a fully covariant, multidimensional transfer equation solver incorporating an adaptive angle or frequency mesh is beyond the scope of the present effort, and remains a subject for future studies.

4.2. *The Method of Short Characteristics*

Having formed a discrete set of $N + C$ tangent planes from the HD mesh, we can now turn to the problem of solving the transfer equation at each value of the polar angle Θ on each plane. The transfer equation written in cylindrical coordinates is

$$\frac{\mu}{\chi}\frac{\partial I}{\partial z} + \frac{\gamma}{\chi}\frac{\partial I}{\partial x} = S - I\,, \tag{51}$$

where γ and μ are the angle cosines on the x- and z-axes, respectively, and $I = I(x, z, \gamma, \mu, \nu)$. We can incorporate a contribution to the source function via scattering using

$$S = (1 - \xi)J + \xi B\,, \tag{52}$$

where $J = (c/4\pi)E$, assuming LTE, and ξ is the destruction probability ($0 < \xi < 1$). For frequency dependent transport, a scattering term in the source function makes the problem much more difficult, as photons can be scattered to different frequencies, producing an implicit coupling between the transfer problem at each frequency. We avoid these difficulties here by solving only the frequency integrated transport problem, using the total (frequency integrated) opacities and source functions.

At each spatial position (x, z) on the radiation grid we wish to solve the transfer equation for a discrete set of rays which sample the full polar angular dependence of I. Along each ray, the transfer equation is

$$\frac{\partial I}{\partial s} = \chi(S - I)\,, \tag{53}$$

where s is a pathlength along the ray measured in the direction of propagation

$$ds = dx/\gamma = dz/\mu\,. \tag{54}$$

There are two methods by which we can compute the specific intensity at each spatial position. The most obvious method we could use would be to project rays from each grid point to the domain boundaries (where the specific intensity is known via boundary conditions), and use interpolation of the physical variables along that ray to solve the transfer problem. This is called the *method of long characteristics.* Since there are N^2 grid points in two dimensions (where N is a measure of the number of grid points on a side), and the number of interpolations on each ray scales as N, then the time to construct the radiation field on the full grid scales as N^3 in two dimensions. For large grids, this can make the method prohibitively expensive. The second method, called the *method of short characteristics,* involves solving the transfer problem only across the cell next to the point under consideration. The contributions of neighboring cells to the physical values are incorporated via interpolations along grid lines. This interpolation can make this method more diffusive than the method of long characteristics; however, this effect can be decreased (to the same order of accuracy as the spatial interpolation used in the HD) by using a high-order interpolation method. Since for each grid cell there is only one ray segment to construct, the time to construct the radiation field on the whole grid scales as only N^2 in two dimensions. For this reason, we have implemented the method of short characteristics in ZEUS-2D to solve the transfer equations, as described below.

Consider a region near the point O in the radiation grid (see Fig. 5). The point M marks the upwind cell boundary on the short characteristic (ray segment) MO. The formal solution of the transfer equation (53) along this short characteristic MO is then

$$I_O = I_M \exp(-\Delta\tau_M) + \int_0^{\Delta\tau_M} dt S(t) \exp[-(\Delta\tau_M - t)]\,, \tag{55}$$

where I_M is the upwind intensity at point M, $S(t)$ is the source function along the ray segment, and $\Delta\tau_M$ is the optical depth between M and O, defined via the path integral

$$\Delta\tau_M = \int_M^O \chi(t)dt\,. \tag{56}$$

The formal solution can be evaluated numerically provided that values for I_M and $\Delta\tau_M$, are known, and a numerical approximation

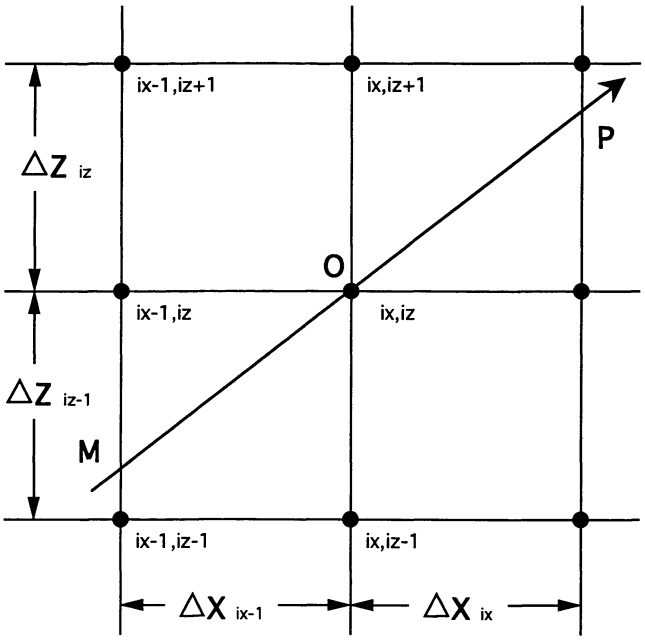

FIG. 5.—Region near a general point O on the radiation grid at which the specific intensity is to be computed with the method of short characteristics. The arrow depicts a ray (drawn for $\mu > 0$) on which the transfer equation is solved. At the upwind point M, quantities must be interpolated from the neighboring grid vertices.

to the integral

$$C_{ij} = \exp(-\Delta\tau_M) \int_M^O S(t) \exp(t) dt \tag{57}$$

can be evaluated.

In general, the upwind point M will not be a grid vertex, even for rectangular meshes, but will lie along either horizontal or vertical mesh lines. Thus the value of the upwind intensity M must be calculated using interpolation between neighboring points at which the intensity is known. Which mesh line is cut by the ray MO depends on the relative sizes of the local grid spacing Δx_{ix} and Δz_{iz}, and the values of the direction cosines γ and μ (which depend on the discrete value of the polar angle Θ). Mihalas, Auer, & Mihalas (1978) and Kunasz & Auer (1988) have described a very efficient test for determining which grid line is cut by the ray MO. Let

$$a_M = \begin{cases} (\gamma \Delta z_{iz-1})/(\mu \Delta x_{ix-1}) & \text{for } \mu > 0 , \\ (\gamma \Delta z_{iz})/(|\mu| \Delta x_{ix-1}) & \text{for } \mu < 0 . \end{cases} \tag{58}$$

Then, if $a_m < 1$, M lies on a horizontal mesh line, and

$$\Delta s_M = \begin{cases} \Delta z_{iz-1}/\mu & \text{for } \mu > 0 , \\ \Delta z_{iz}/\mu & \text{for } \mu < 0 , \end{cases} \tag{59}$$

$$I_M = \begin{cases} (1 - a_M) I_{ix,iz-1} + a_M I_{ix-1,iz-1} & \text{for } \mu > 0 , \\ (1 - a_M) I_{ix,iz+1} + a_M I_{ix-1,iz+1} & \text{for } \mu < 0 , \end{cases} \tag{60}$$

while if $a_m > 1$, M lies on a vertical mesh line, and

$$\Delta s_M = \Delta x_{ix-1}/\gamma , \tag{61}$$

$$I_M = \begin{cases} (1 - 1/a_M) I_{ix-1,iz} + (1/a_M) I_{ix-1,iz-1} & \text{for } \mu > 0 , \\ (1 - 1/a_M) I_{ix-1,iz} + (1/a_M) I_{ix-1,iz+1} & \text{for } \mu < 0 , \end{cases} \tag{62}$$

where Δs_M is the physical path length along MO. We have used a linear interpolation formula to compute I_M, the advantage of

which is that only two neighboring grid vertices are needed for the interpolation. However, the interpolations intrinsic to the method of short characteristics introduce angular diffusion into the numerical solution for the radiation field; sharp gradients in the specific intensity will spread over neighboring points in the downwind direction. Kunasz & Auer (1988) have demonstrated that a parabolic interpolation formula reduces this diffusion, providing a more accurate result. However, not only is the parabolic interpolation more complex (requiring three upwind interpolation points), but it also can introduce unphysical overshoots of the interpolated quantities near discontinuities in the specific intensity. When I drops rapidly to zero, these overshoots can lead to values for I_M which are less than zero, which are clearly unphysical. These problems are very suggestive of those encountered in the interpolation algorithms used for Eulerian advection schemes. In this case, over and undershoots are eliminated by monotonization, while parabolic interpolation algorithms, including steepeners for regions near discontinuities, are well developed. It therefore seems very likely that a very robust interpolation algorithm for the radiation variables along grid lines could be built using methods analogous to those required for Eulerian advection.

The optical depth along the ray segment $\Delta\tau_M$ can be approximated by assuming that ln (χ) is a piecewise linear function along the ray (Mihalas et al. 1978). Thus

$$\ln \chi = \ln \chi_M + \beta(S_M - S_O)/\Delta s_M , \tag{63}$$

where $\beta = \ln (\chi_M/\chi_O)$. Then

$$\Delta\tau_M = \int_M^O \chi(s)ds = (\chi_O - \chi_M)\Delta s_M/\beta . \tag{64}$$

For $\beta \ll 1$, we use an approximation based on the Euler-MacLaurin summation formula, which gives eventually

$$\Delta\tau_M = \frac{1}{2}\Delta s_M\left[\chi_O + \chi_M - \frac{\beta}{6}(\chi_O - \chi_M)\left(1 - \frac{\beta^2}{60}\right)\right] . \tag{65}$$

Similarly, the source integral C_{ij} can be evaluated approximately assuming the source function is a piecewise linear function along the ray. Then

$$C_{ij} = \Psi_M S_M + \Psi_O S_O , \tag{66}$$

where the weights are

$$\Psi_M = (1 - e^{-\Delta\tau_M})/\Delta\tau_M - e^{-\Delta\tau_M} ,$$

$$\Psi_O = 1 - (1 - e^{-\Delta\tau_M})/\Delta\tau_M ,$$

and S_M is the source function at M formed by linear interpolation along mesh lines (much like I_M), and S_O is known since O is a vertex. For very small optical depth, the weights can be expanded using a Taylor series so that

$$\Psi_M = (1 - e^{-x})/x - e^{-x} \approx x(\tfrac{1}{2} - \tfrac{1}{3}x + \tfrac{1}{8}x^2 - \cdots) , \tag{67}$$

$$\Psi_O = 1 - (1 - e^{-x})/x \approx \tfrac{1}{2}x(1 - \tfrac{1}{3}x + \tfrac{1}{12}x^2 - \cdots) . \tag{68}$$

Since we have used linear interpolation for the upwind intensity and source functions, the numerical formula we use can be written in full as

$$I_O = I_M \exp(-\Delta\tau_M) + S_O - S_M \exp(-\Delta\tau_M) + \frac{S_O - S_M}{\Delta\tau_M}[1 - \exp(-\Delta\tau_M)] . \tag{69}$$

When written in this form, it can be easily seen that this formula gives the correct limits for both very large optical depth ($I_O \approx S_O$, the diffusion approximation), and for very small optical depths [$I_O = I_M + (S_O - S_M)$]. In the absence of internal sources, we also find the correct exponential attenuation, $I_O = I_M e^{-\Delta\tau}$. Thus, we see that equation (69) is able to provide a stable determination for I_O, which will always be positive, and reduces to the correct limits.

However, the interpolation formula for I_M masks the primary difficulty in efficient numerical implementation of the short characteristic method. Since, in order to perform the interpolation, the intensity must be known at two upwind vertices, the short characteristics formula is recursive. For positive μ, the solution over the entire mesh must be built up by sweeping along rows or columns, starting from the lower left corner and moving away from the known boundary values along the bottom and left edges. For negative μ, the solution is built up by sweeping along rows or columns starting from the upper left corner and moving away from

known boundary values along the left and top edges. While sweeping along rows or columns in this manner avoids unresolved dependencies, it results in an unvectorizable algorithm. However, the method can be vectorized if one sweeps along *diagonals* of the mesh (from the lower left to upper right for $\mu < 0$ and from lower right to upper left for $\mu > 0$). This results in a very efficient algorithm.

Once the radiation field at a given polar angle μ is constructed over the entire radiation grid the process is repeated for each discrete μ value at which the radiation field is sampled. After all μ values are completed, we solve the transfer problem on successive tangent planes until all tangent planes are completed. The full spatial and angular dependence can then be assimilated to form the angular moments, and thus the Eddington factors.

4.3. *Computing the Eddington Factors*

The primary purpose of the formal solution of the transfer equation in the radiation module is to compute the full angular dependence of the radiation field at every HD grid point, so that the Eddington factors can be computed from angular moments. (The transfer equation solver can also be used as a graphical post processor to compute the emergent intensity from a simulation). We describe this process below.

In cylindrical coordinates, the unit vector marking the direction of propagation of the radiation field can be written as (see Fig. 3)

$$\boldsymbol{n} = \sqrt{1-\mu^2}\cos\Phi\hat{r} + \sqrt{1-\mu^2}\sin\Phi\hat{\Phi} + \mu\hat{z}\,, \tag{70}$$

where $\mu = \cos\Theta$. Thus, the angular moments of the radiation field needed to compute all nonzero components of the tensor Eddington factor in two dimensions are

$$E = \frac{1}{c}\oint I(\boldsymbol{n})d\omega = \frac{1}{c}\int_0^{2\pi}\int_{-1}^{1} I(\mu,\Phi)d\mu d\Phi\,, \tag{71}$$

$$P_{zz} = \frac{1}{c}\oint I(\boldsymbol{n})n_z n_z d\omega = \frac{1}{c}\int_0^{2\pi}\int_{-1}^{1} I(\mu,\Phi)\mu^2 d\mu d\Phi\,, \tag{72}$$

$$P_{rz} = \frac{1}{c}\oint I(\boldsymbol{n})n_r n_z d\omega = \frac{1}{c}\int_0^{2\pi}\int_{-1}^{1} I(\mu,\Phi)\sqrt{1-\mu^2}\mu\cos\Phi\, d\mu d\Phi\,, \tag{73}$$

$$P_{rr} = \frac{1}{c}\oint I(\boldsymbol{n})n_r n_r d\omega = \frac{1}{c}\int_0^{2\pi}\int_{-1}^{1} I(\mu,\Phi)(1-\mu^2)\cos^2\Phi d\mu d\Phi\,. \tag{74}$$

We have already described, in § 4.1, how the radiation grid is constructed to resolve the specific intensity in both space and angle. The polar angular variation is resolved by a discrete set of rays which sample the full range $0 \le \Theta \le \pi$ ($1 \le \mu \le -1$). If the problem possesses equatorial symmetry, then rays with $\mu > 0$ above the symmetry plane ($z > 0$) are equivalent to rays with $\mu < 0$ below the symmetry plane, Thus, for problems with equatorial symmetry, we only need rays which span the range $0 \le \Theta \le \pi/2$ ($1 < \mu < 0$). In principle, we can choose any set of Θ for the rays, but in practice the set which is equally spaced in solid angle [i.e., $\cos(\Delta\Theta) = constant$] is used most often. The azimuthal angular variation is resolved by the intersections of a given radial shell with different tangent planes. Each shell will intersect a given tangent plane twice, once for incoming rays ($\pi/2 < \Phi < \pi$) and once for outgoing rays ($0 < \Phi < \pi/2$). This generates discrete Φ values in the domain ($0 \le \Phi \le \pi$); values for ($-\pi \le \Phi \le 0$) are given by axisymmetry. Thus, we see that the intersection of radial shells and tangent planes will resolve the radiation field over the entire domain ($-\pi \le \Phi \le \pi$). Unfortunately, however, we have no control over what values of Φ the radiation field is sampled at. The discrete values of Φ are determined entirely by the geometry of the tangent planes and shells.

Given a set of specific intensity values sampled at discrete μ and Φ values [i.e., $I_{i,j} = I(\mu_i, \Phi_j)$], then we can use numerical quadratures to approximate the angular moments (eqs. [71]–[74]). Thus we can write

$$E = \frac{1}{c}\int_0^{2\pi} d\Phi \int_{-1}^{1} d\mu I(\mu,\Phi) = \sum_j W1_j\left(\sum_i W2_i I_{i,j}\right), \tag{75}$$

$$Pzz = \frac{1}{c}\int_0^{2\pi} d\Phi \int_{-1}^{1} d\mu\mu^2 I(\mu,\Phi) = \sum_j W3_j\left(\sum_i W4_i I_{i,j}\right), \tag{76}$$

$$Prz = \frac{1}{c}\int_0^{2\pi} d\Phi\cos\Phi \int_{-1}^{1} d\mu\sqrt{1-\mu^2}\mu I(\mu,\Phi) = \sum_j W5_j\left(\sum_i W6_i I_{i,j}\right), \tag{77}$$

$$Prr = \frac{1}{c}\int_0^{2\pi} d\Phi\cos^2\Phi \int_{-1}^{1} d\mu(1-\mu^2) I(\mu,\Phi) = \sum_j W7_j\left(\sum_i W8_i I_{i,j}\right), \tag{78}$$

where the $W1, W2, \ldots, W8$ are the weights for the various integrals. To compute these weights, we assume that $I(\mu, \Phi)$ is a separable, piecewise linear function of μ and $\cos\Phi$ *within a cell,* so that

$$I(\mu, \Phi) = I(\mu)I(\Phi) = \left[I_{i-1} + \frac{I_i - I_{i-1}}{\Delta\mu}(\mu - \mu_{i-1})\right]\left[I_j + \frac{I_j - I_{j-1}}{\Delta\cos\Phi}(\cos\Phi - \cos\Phi_{j-1})\right]. \quad (79)$$

By substituting equation (79) into equations (75)–(78), the integrals can be performed analytically, yielding expressions for the weights. Then, by choosing a discrete set of μ and Φ values at which to sample the radiation field initially the weights can be computed once and for all at the start of the simulation.

The formulae for the weights are quite complex, and accurate coding of them is a concern. We can perform a numerical check on the weights computed in the code by calculating the test integrals

$$I_1 = \int_0^{2\pi} d\Phi = 2\pi = \sum_j W1_j = \sum_j W3_j, \quad (80)$$

$$I_2 = \int_0^{2\pi} \cos\Phi d\Phi = 0 = \sum_j W5_j, \quad (81)$$

$$I_3 = \int_0^{2\pi} \cos^2\Phi d\Phi = \pi = \sum_j W7_j, \quad (82)$$

$$I_4 = \int_{-1}^{1} d\mu = 2 = \sum_i W2_i, \quad (83)$$

$$I_5 = \int_{-1}^{1} \mu^2 d\mu = \tfrac{2}{3} = \sum_i W4_i, \quad (84)$$

$$I_6 = \int_{-1}^{1} \sqrt{1-\mu^2}\mu d\mu = 0 = \sum_i W6_i, \quad (85)$$

$$I_7 = \int_{-1}^{1} (1-\mu^2) d\mu = \tfrac{4}{3} = \sum_i W8_i. \quad (86)$$

Thus, whenever, the quadrature weights are initialized at the start of a simulation, we perform the test integrals in equations (80)–(86) to ensure they have been computed properly. In practice, we have found that the numerical evaluation of the test integral agrees with the analytic results to at least one part in 10^6, even when only a few discrete μ or Φ values are used.

In practice, computing the four-dimensional specific intensity for all space angle mesh points before starting the quadratures (eqs. [75]–[78]) would require large amounts of memory. Thus, after computing the specific intensity of a given tangent plane, we do not save it, but sum it directly into the quadratures. The quadratures are completed only after solving the radiation field for every ray on every tangent plane. The components of the tensor Eddington factor can then be computed directly from equation (16). Since the radiation field (and thus the quadratures) are all zone centered, whereas the Eddington factors are centered at the same positions as the corresponding pressure tensor components, equation (16) can be differenced as

$$f11_{i,j} = Pzz_{i,j}/E_{i,j}, \quad (87)$$

$$f22_{i,j} = Prr_{i,j}/E_{i,j}, \quad (88)$$

$$f12_{i,j} = \frac{Prz_{i-1,j} + Prz_{i,j} + Prz_{i-1,j-1} + Prz_{i,j-1}}{E_{i-1,j} + E_{i,j} + E_{i-1,j-1} + E_{i,j-1}}. \quad (89)$$

Finally, boundary conditions are applied to the Eddington factors which are consistent with those implied for the radiation energy density and pressure (i.e., either reflecting, inflow or outflow). The Eddington factors can then be used in the next solution of the radiation moment equations to update the dynamical variables.

5. MODIFYING ZEUS-2D TO INCORPORATE THE RADIATION MODULE

While the moment equation solver (described in § 3) and the transfer equation solver (described in § 4) are quite complex internally, they nonetheless are self-contained modules which can easily be incorporated into the ZEUS-2D code. Figure 6 shows

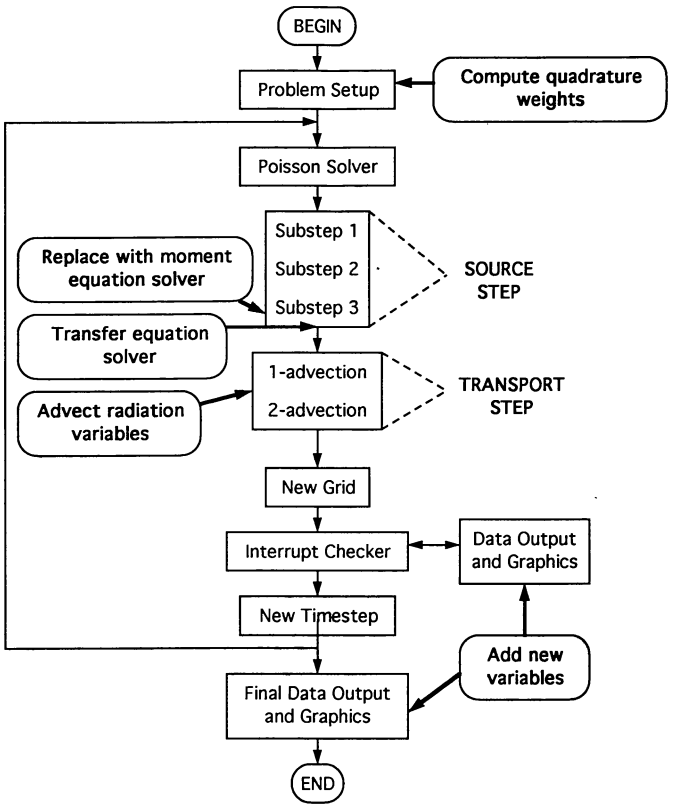

FIG. 6.—Schematic flow chart of the ZEUS-2D code which diagrams the changes required to add the RHD algorithms to the HD algorithms. Compare this figure to Fig. 7 of Paper I.

how the schematic flow chart for the code, originally presented in Figure 7 of Paper I, is altered when the radiation module is included. The significant changes are that "Substep 3" of the source step (which originally performed the compressional heating of the material energy density) is now replaced by the moment equation solver described in § 3.2. Directly after the solution of the moment equations, the transfer equation solver is called to update the components of the tensor variable Eddington factors to be used in the next cycle as described in § 4. The transport step must also be modified to advect the radiation variables across the grid as described in § 3.3. Finally an additional routine must be added to the setup to compute the quadrature weights, and of course changes must be made to the graphics routines to add output of the new variables.

We use the precompiler CPP to control the incorporation of the radiation module into the ZEUS-2D code. All routines and variables needed by the radiation module are labeled by a conditional macro, and thus optimized versions of the code can be generated both with and without reference to the RHD.

As a consequence of solving the transfer equation to compute the Eddington factor, the radiation module is able to compute the emergent radiation field from the object under study. The emergent intensity is probably the most relevant quantity to compare to observations, since it is directly analogous to what would be observed by an Earth-based telescope. We can exploit this capability by using the transfer equation solver as a graphical post processor, to compute maps of the emergent intensity from any simulation (even if radiation was not used to compute the dynamics of the simulation). Indeed, this capability is a strong motivation to develop more sophisticated versions of the transfer equation solver, which can account for frequency dependent transport in a moving media (to allow the calculation of line profiles for comparison with observations).

6. TESTS OF THE MOMENT EQUATION SOLVER

Having described the implementation of the moment and transfer equation solvers in ZEUS-2D, we can now present the results of the test problems we have used to verify our algorithms. However, there are very few two-dimensional RHD calculations which are suitable for use as test problems. Thus, much like the MHD algorithms, we have found it necessary to design our new collection of test problems for the RHD algorithms. Since the moment and transfer equations solvers are independent modules, we can test each separately. In this section, we begin by describing tests of the solution of the moment equations.

The radiation moment equations have a completely different mathematical behavior in each of three different physical regimes (the streaming limit, the static diffusion limit, and the dynamic diffusion limit) as described in § 3. By making the appropriate choices for the material properties and fluid velocity, we can test the moment equation solver in each of these three limits, thereby demonstrating the algorithms can produce the correct results in any physical regime. Below we present three such test problems.

6.1. *A Streaming Limit Test*

We can set up a streaming limit test by choosing χ_F and Δt such that $c\chi_F\Delta t \ll 1$ and setting the Eddington factors in the direction of propagation to 1.0, while all other components are zero. We showed in § 3 that the radiation energy equation becomes an advection equation in this case, with features propagated across the grid at the speed of light. For this problem, we introduce a discontinuity in radiation energy density at $t = 0$ by setting a nonzero flux at the left boundary, and then follow the square wave as it crosses a grid of 100 zones. This problem is identical to one performed by Mihalas & Klein (1982) and Stone & Mihalas (1991). Figure 7 shows the results for the radiation energy density and flux using two different time centering schemes. In both cases we choose a time step such that $(c\Delta t)/(\Delta x) = 2$, but in the top panels of the figure we have chosen the time centering parameter θ used in the time centering of the RHS of the moment equation (see §§ 3 and 2) to be $\theta = 1.0$, while in the bottom panels of the figure we have used $\theta = 0.5$. In the former case the temporal differencing scheme is fully implicit, while in the latter it is Crank-Nicholson. We find that the fully implicit scheme gives a smooth representation of the front with the correct velocity c, but that it is quite diffusive. The Crank-Nicholson differencing, while less diffusive, introduces unphysical oscillations behind the front which are slowly damped away. Mihalas & Klein (1982) also observed these oscillations, but since their scheme was conservative they were not damped. Stone & Mihalas (1991) have described a scheme appropriate for the solution of the time-dependent transfer equation which does not introduce oscillations. Such oscillations could have serious consequences for dynamic simulations, as the material

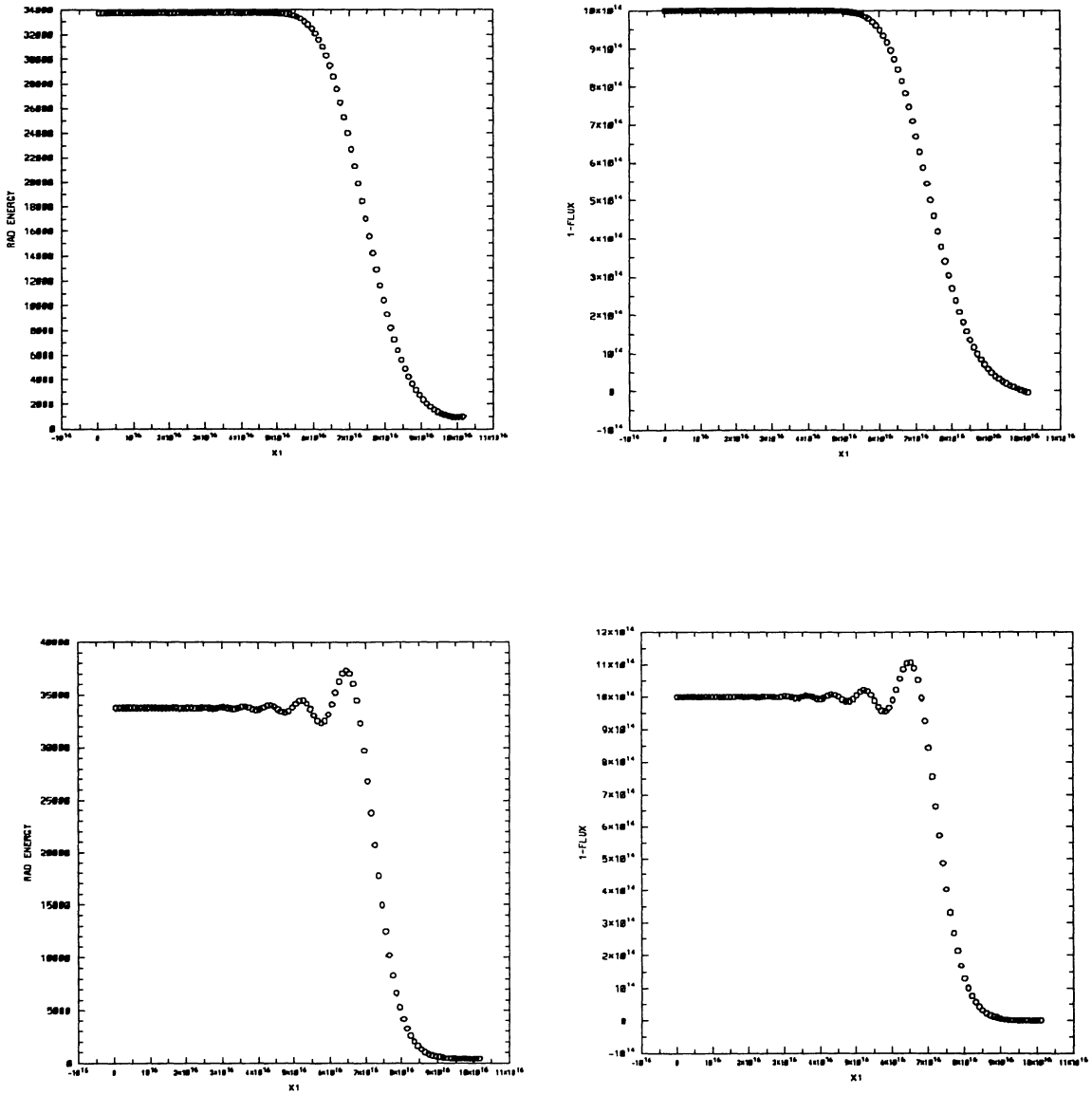

FIG. 7.—Results for the propagation of a step function of radiation energy density in an optically thin fluid (streaming limit test). The analytic position of the radiation front is given by $ct = 7.5 \times 10^{16}$. (*top*) Radiation energy density (*left*) and flux (*right*) using fully implicit time differencing. (*bottom*) Radiation energy density (*left*) and flux (*right*) using Crank-Nicholson time differencing. One hundred grid points are used in both cases.

properties behind the front would also undergo large fluctuations. Thus, although more diffusive, the fully implicit scheme is clearly the better of the two.

We have also performed this test for fully implicit time differencing ($\theta = 1.0$) with a larger time step, so that $(c\Delta t)/(\Delta x) = 4$. The results at the larger time step compare very favorably with those in Figure 7.

6.2. *A Static Diffusion Limit Test*

The diffusion limit implies $c\chi_F \Delta t \gg 1$, and the radiation field is isotropic so that the Eddington factors are $f_{ii} = \frac{1}{3}$ and $f_{ij} = 0$ for $i \neq j$. In the static diffusion limit, the characteristic diffusion time for the radiation field ($\Delta t \sim [\Delta x]^2/4D$ where $D \approx c/3\chi_F$) is much smaller than an advection time scale set by fluid motion ($\Delta t \sim \Delta x/v$). Therefore, to setup a static diffusion limit test we can initialize a strongly peaked distribution of radiation energy density (such as a Gaussian) in a motionless fluid, initialize the Eddington factors as above, and follow the evolution of the pulse as it diffuses away. An attractive feature of a Gaussian pulse is that the time evolution is described by an analytic solution, which gives that the amplitude of the pulse follows $A(t) = A_0 t^{-1/2}$. A Gaussian pulse therefore provides a quantitative test.

For this problem we initialize the pulse at the origin of a 20×20 grid in Cartesian geometry. We use reflecting boundary conditions everywhere, and follow the evolution for several diffusion times. Figure 8 presents the results for the radiation energy density and flux from two tests, one with an effective diffusion constant $D \approx 1$, and the other with $D \approx 100$. In the first case, We follow the evolution for ~ 1.0 diffusion times, so that the amplitude of the Gaussian drops by a factor of 4. Notice in this case that the pulse remains spherical and smooth, and that the flux is symmetric for this two-dimensional problem. We find that the amplitude of the pulse agrees with the analytic time evolution to within 4% over the entire evolution, even for this relatively coarse grid. In the second case, we follow the evolution for much longer, ~ 100 diffusion times, so that now the variation of the energy density over the whole grid is now only 4.0×10^{-3}. We find that the contours of the energy density take on the correct characteristic pattern implied by the reflecting boundary conditions, and that the flux is again everywhere smooth and symmetric over the whole two-dimensional grid. If we follow the evolution further, to ~ 1000 diffusion times, we find qualitatively the same result except now the variation in the energy density is only one part in 10^{10}!

6.3. *A Dynamic Diffusion Limit Test*

For this problem, we now choose the advection time to be much shorter than the diffusion time by setting up a Gaussian pulse in a *moving* fluid. Using a 64×64 grid in Cartesian geometry, we initialize the pulse in the lower left corner, and using velocities of equal magnitude in both the 1- and 2-directions, we advect it to the upper right corner. We choose the opacities and velocities such that the diffusion time scale is $\sim 10^{-4}$ the advection time scale. Figure 9 shows the results of this test using the van Leer advection algorithm. We find that the pulse shape has become slightly square, but the contours remain smooth, and the flux is qualitatively correct, following the gradients of the energy density very well. The "squaring-up" of the pulse is undoubtedly due to the directionally split advection algorithm we use in multidimensions; we expect the same results for the two-dimensional advection of all the other variables as well. The pulse amplitude has decreased substantially, however this too is attributable to the diffusion of the advection algorithm. With such a coarse grid, only five zones are centered in the peak of the pulse initially; thus we expect the diffusion in the advection algorithm to be strong. Indeed, we have found that we can substantially decrease the diffusion of the pulse using PPA instead of the van Leer algorithm.

7. TESTS OF THE TRANSFER EQUATION SOLVER

There are two important steps in the transfer equation solver: (1) using the method of short characteristics to compute the radiation field on a given radiation grid for a particular polar angle μ, and (2) assimilating all of the angular information about the radiation field over all the tangent planes and rays to compute the Eddington factor. We present the results from tests of both steps below.

7.1. *Searchlight Beam Test*

This popular test of multidimensional transfer algorithms has been used by Kunasz & Auer (1988) and others. It involves introducing a narrow beam of radiation into a radiation grid at a specific polar angle, and computing the distribution of intensity over the whole grid. For an optically thin medium with no sources, the beam should propagate across the grid with no dispersion or attenuation.

We present results for this test in Figure 10. We use both a 16×16 grid and a 64×64 grid, and introduce the beam at the lower (or upper) corner using polar angles of $+45°$ (or $-45°$). The grid is not square, so that the radiation field will not propagate along vertices. We find there is considerable diffusion as the beam propagates across the mesh (due to the linear interpolation inherent in our method) which results in some attenuation along the beam center. This diffusion decreases substantially, however, with a finer grid. Moreover, the results for positive and negative μ are precisely symmetric. These results are essentially identical to those presented by Kunasz & Auer (1988).

7.2. *Linear Source Function Test*

We can design a much more quantitative test of the method of short characteristics by initializing the opacity and source function

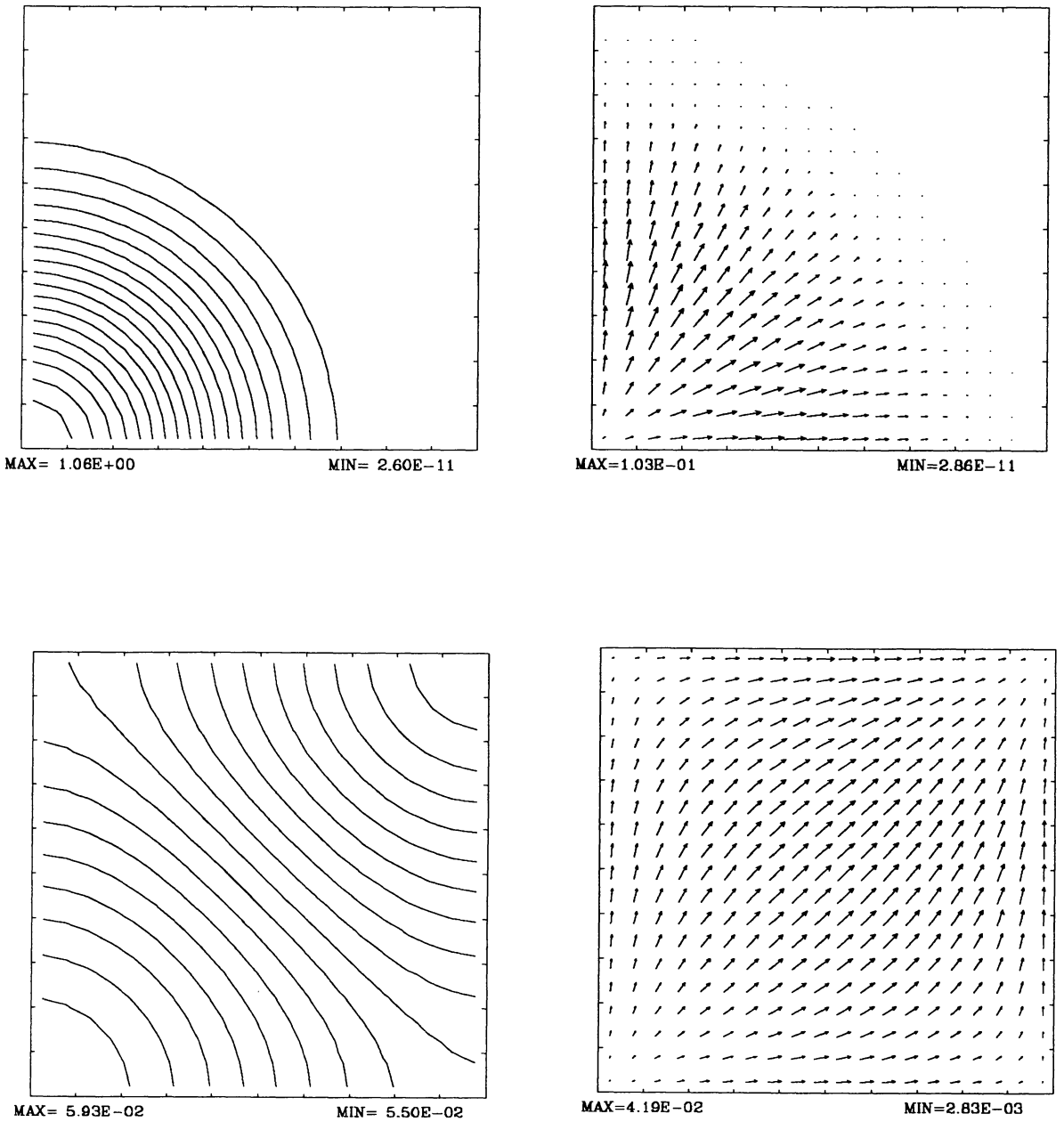

FIG. 8.—Results for the diffusion of a Gaussian pulse of radiation energy density in a stationary fluid (static diffusion limit test). (*top*) Radiation energy density (*left*) and flux (*right*) using an effective diffusion constant of $D = 1$ shown at roughly one diffusion time. (*bottom*) Radiation energy density (*left*) and flux (*right*) using an effective diffusion constant of $D = 100$ shown at roughly 100 diffusion times. In this case, the contours and vectors take on a pattern characteristic for the reflecting boundary conditions imposed.

to be linear functions of the path length along a ray, so that $S(t) = S_0 + S_1 t$ and $\chi(t) = \chi_0 + \chi_1 t$. In this case, the transfer equation (53) has a simple analytic solution

$$I(t) = I_0 e^{-\Delta\tau} + S_0(1 - e^{-\Delta\tau}) + S_1[(\Delta\tau - 1) + e^{-\Delta\tau}] , \tag{90}$$

where

$$\Delta\tau = \int_{l_0}^{l_1} (\chi_0 + \chi_1 t)dt = \chi_0(l_1 - l_0) + \chi_1(l_1 - l_0)(l_1 + l_0)/2 . \tag{91}$$

Since we are using linear functions to represent the variation of physical variables in this problem, the linear interpolation used in our implementation of the method of short characteristics should be exact.

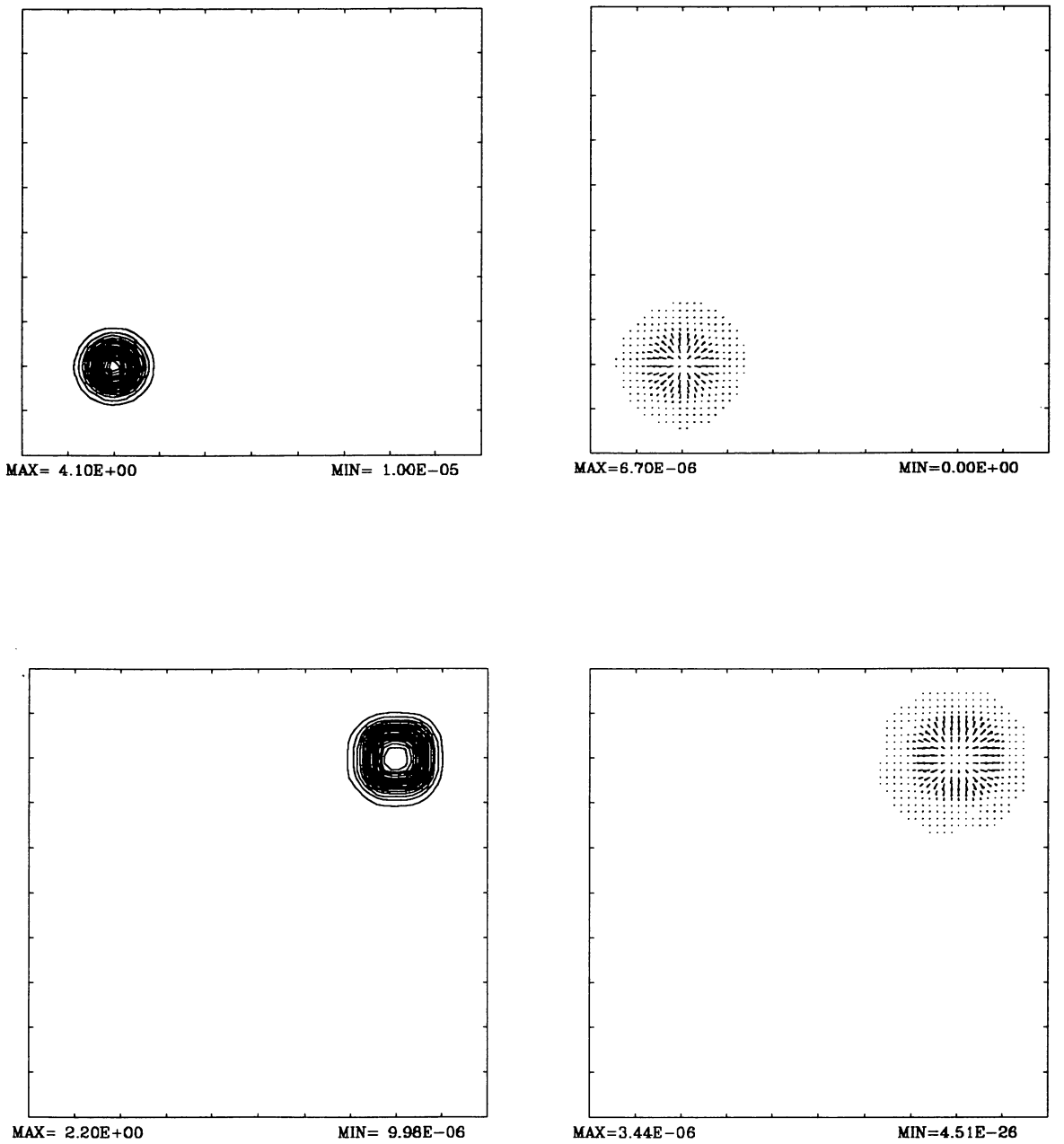

FIG. 9.—Results for the diffusion of a Gaussian pulse of radiation energy density in a moving fluid (dynamic diffusion limit test). (*top*) Radiation energy density (*left*) and flux (*right*) initially. (*bottom*) Radiation energy density (*left*) and flux (*right*) after the pulse has been advected across the grid.

We present the results from two tests, one in which the source function is constant ($S_0 = 1, S_1 = 0$), and the other in which the source function is linear ($S_0 = 1, S_1 = 1$), see Figure 11. We present contour plots of the specific intensity and the error relative to the analytic solution in both cases. We set $I_0 = 2$, $\chi = constant = 1.0$, and $\mu = \frac{2}{9}$, and have used grids of 64×32 in each test. In both cases, the error is dominated by a diagonal band stretching from the lower corner and extending to the top. This band marks the location where the slope of the specific intensity is discontinuous when measured across rows or columns, since the path length to the boundary for adjacent zones is not constant to the left of the diagonal. Linear interpolation across the discontinuity in the slope of the specific intensity generates the error. Even so, the largest error on the grid is only 1.92% for the constant source function test, and 1.64% for the linearly varying source function test. For the former problem, the error is not confined solely to the diagonal band, but some error contours also appear to the left. These arise because the specific intensity is actually varying exponentially along rows in this region, thus linear interpolation does not give an exact result. We find, however, that for both tests, the specific intensity agrees with the analytic result to machine round off error in the region to the right of the diagonal band, as we expect.

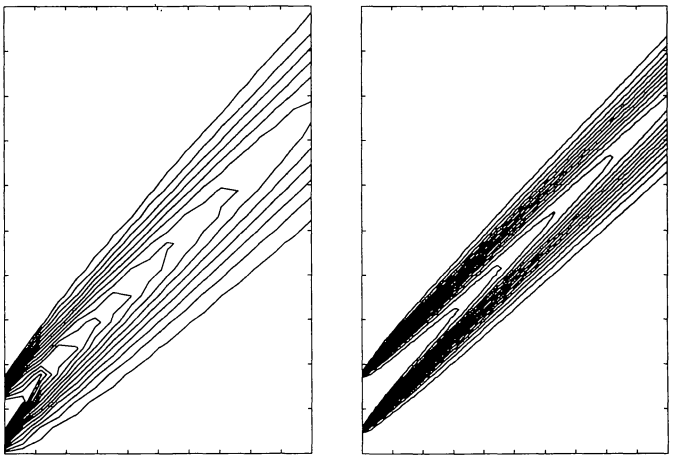

FIG. 10.—Contours of the specific intensity on a given tangent plane from the search light beam test for grids of 16×16 (*left*) and 64×64 (*right*) and $\mu > 0$. Analytically the beam should propagate directly across the mesh with no diffusion or dispersion.

7.3. *Tests of the Eddington Factors*

Computing the Eddington factors requires assimilating the correct angular variation of the radiation field, and then performing the appropriate numerical quadratures. We mentioned, in § 4.3, that we performed test integrals using the quadrature weights to ensure the latter are computed and stored correctly. Since two-dimensional analytic solutions to the transfer equation, including a description of the full angular distribution of the radiation field, are difficult to compute, finding additional *quantitative* checks of the Eddington factors is difficult. We have therefore used the following *qualitative* tests.

The simplest check is to compute the Eddington factors for the radiation field in a cylinder in thermal equlibrium, with isotropic boundary conditions. Since the radiation field should be isotropic everywhere, we expect $f_{ii} = \frac{1}{3}$ and $f_{ij} = 0$ for $i \neq j$. We find that the transfer equation module reproduces these results everywhere to the limit set by machine round-off error. If this test is repeated using zero incident radiation at the boundaries, we expect the radiation field to be mostly axial at the top and bottom of the cylinder (so $f_{11} \rightarrow 1$ there), and mostly radial at the edges (so $f_{22} \rightarrow 1$ there). Figure 12 shows the results in the case, for a cylinder of length

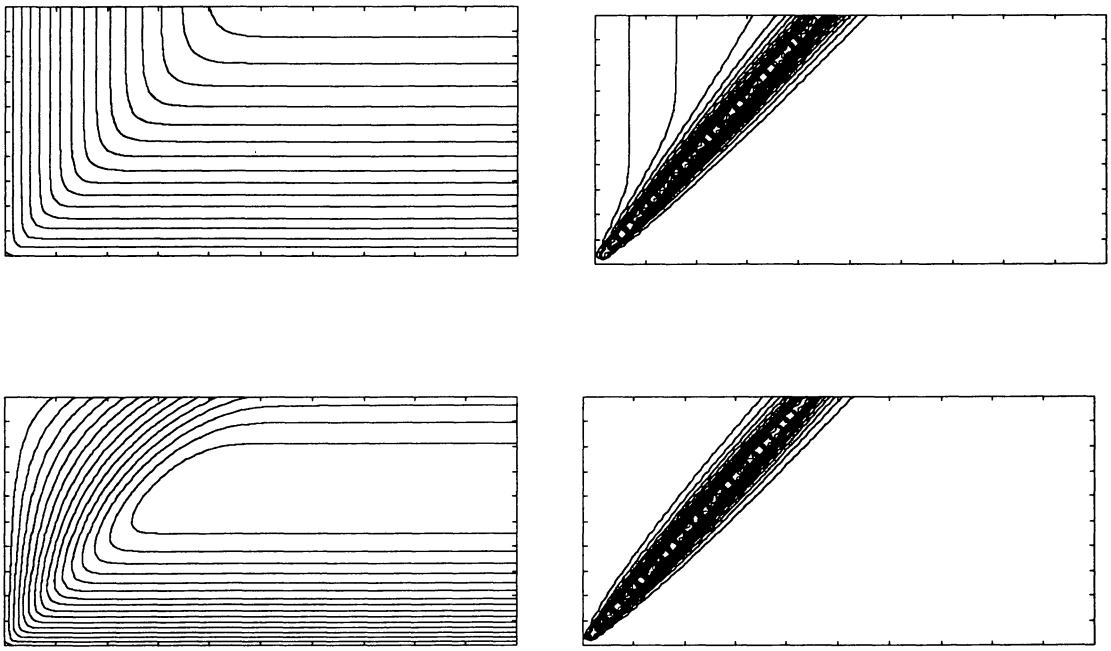

FIG. 11.—Results of the linear source function test of the transfer equation solver. Radiation is introduced along the lower and left boundaries at $\mu = \frac{2}{9}$ into a grid in which the source function is either constant or varies linearly along the rays. (*top*) Contours of the specific intensity (*left*) and errors in the specific intensity (*right*) for a constant source function. The maximum error is 1.92%. (*bottom*) Contours of the specific intensity (*left*) and errors in the specific intensity (*right*) for a linearly varying source function. The maximum error is 1.64%.

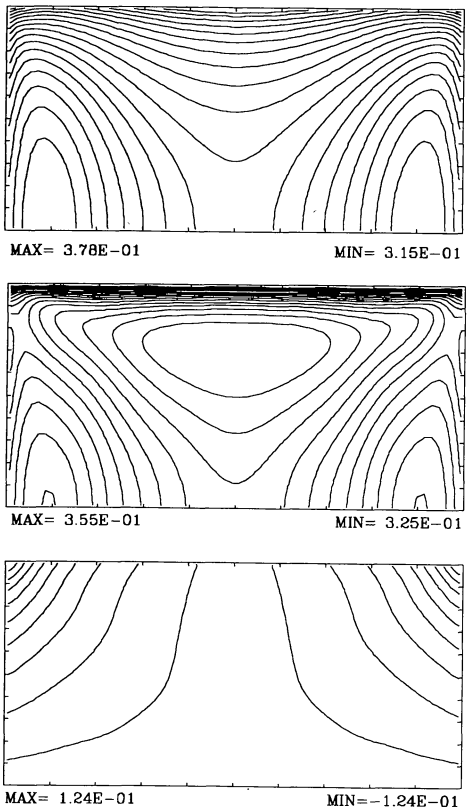

FIG. 12.—f_{11} (*top*), f_{22} (*middle*), and f_{12} (*bottom*) components of the tensor Eddington factor for a cylinder with optical depth two along its length and diameter in thermal equilibrium with zero incident radiation on its boundaries. The Z-axis is plotted horizontally, the R-axis vertically. The lower boundary is the axis of symmetry. The solution shows the correct qualitative behavior, with $f_{11} > \frac{1}{3}$ along the axis, and $f_{22} > \frac{1}{3}$ off-axis. Sixteen equally spaced contours between the minimum and maximum are shown.

$Z = 2$, and radius $R = 1$, with $\chi = 1$ so that the optical depth either across a diameter or parallel to the axis of symmetry is 2.0. Figure 12 shows qualitative agreement with our expected results, i.e., f_{11} is a maximum on axis, while f_{22} is a maximum off axis.

Extending the philosophy of the last test, we can compute the Eddington factors for a radiation field which is strongly peaked in either the z or r directions in an optically thin cylinder. The results for both of these cases is shown in Figures 13 and 14, respectively. We again find quantitative agreement with our expected results, i.e., $f_{11} > f_{22}$ in Figure 13 while $f_{22} > f_{11}$ in Figure 14 and all contours are symmetric about the midplane. The interesting result, however, is that f_{12} is negative over some of the domain in both cases. In retrospect, this is actually quite correct; one can deduce from equation (73) that it can occur whenever the radiation field is strongly peaked near $\mu \pm 1$ or $\Phi = \pm\pi$.

8. SUMMARY

In this final paper of the series, we have given a detailed description of the RHD algorithms in the ZEUS-2D code. These algorithms use a tensor variable Eddington factor, computed from a solution of the static transfer equation, to close the system of radiation moment equations. This full transport algorithm, which differs significantly from more commonly used methods based on the diffusion approximation, is therefore applicable in both optically thin and thick media.

We have also presented the results computed by our algorithms on a new collection of RHD test problems. To test the moment equations, we have used tests in each physical regime of the equations, and shown that the correct solution is obtained in each case. The streaming limit test (propagation of a radiation front at the speed of light) is particularly significant, since it shows our algorithms are accurate and stable even for optically thin regions, which is often not true for methods based on the diffusion approximation. Since the moment equation module works well in each different physical regime, we are confident we will be able to treat flows in which the physical conditions are widely disparate in different regions on the grid (such as an optically thick accretion disk surrounded by an optically thin corona and wind).

For the transfer equation, very detailed tests are possible which compare the numerical solution for the specific intensity at every point on a given tangent plane to a known analytic solution. These tests show that while the interpolation inherent in the method of short characteristics makes the solution diffusive, it is not overly so. The function of the transfer equation solver when coupled to the HD is primarily to compute Eddington factors; tests of this latter step in two dimensions are much more difficult to formulate. However, for certain restricted geometries and physical conditions, we find our methods reproduce the expected results either

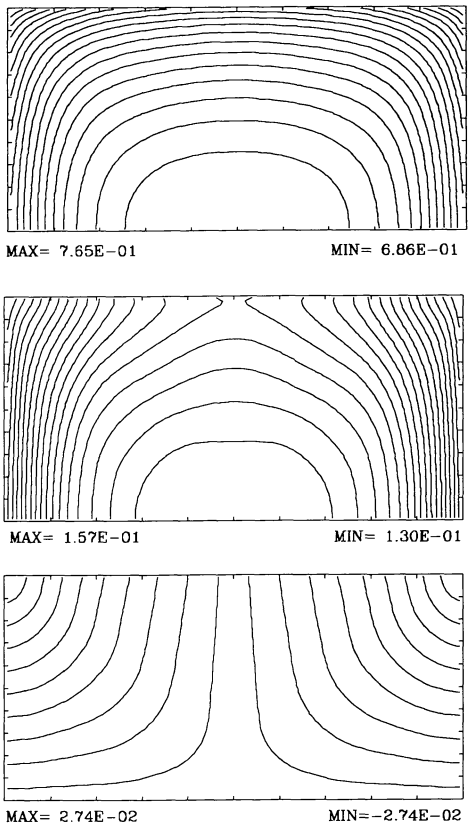

FIG. 13

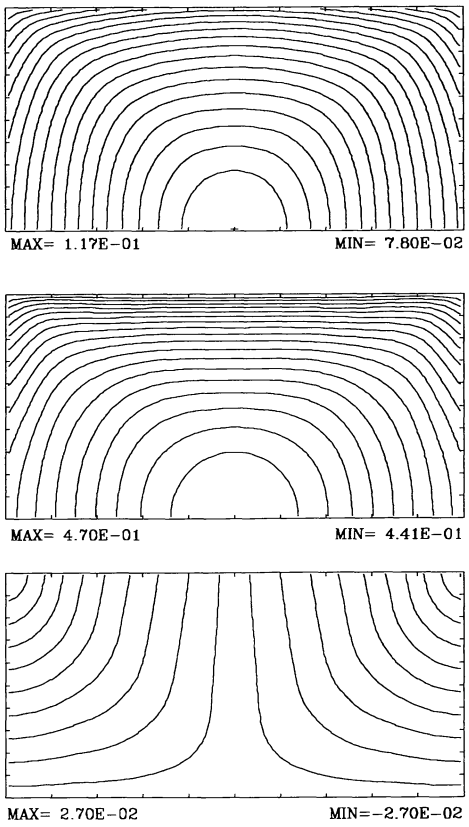

FIG. 14

FIG. 13.—f_{11} (*top*), f_{22} (*middle*), and f_{12} (*bottom*) components of the tensor Eddington factor for an optically thin cylinder with a beamed radiation field propagating along the Z-axis. The Z-axis is plotted horizontally, the R-axis vertically. The lower boundary is the axis of symmetry. The solution shows the correct qualitative behavior, with $f_{11} \gg f_{22}$. Sixteen equally spaced contours between the minimum and maximum are shown.

FIG. 14.—f_{11} (*top*), f_{22} (*middle*), and f_{12} (*bottom*) components of the tensor Eddington factor for an optically thin cyclinder with a beamed radiation field propagating along the R axis. The Z-axis is plotted horizontally, the R-axis vertically. The lower boundary is the axis of symmetry. The solution shows the correct qualitative behavior, with $f_{22} \gg f_{11}$. Sixteen equally spaced contours between the minimum and maximum are shown.

identically (as for a thermal radiation field) or qualititively (as for a beamed radiation field along either axis). The latter test demonstrates the interesting result that the off-diagonal components of the tensor Eddington factor can be negative in some cases, a situation that flux-limited diffusion methods cannot reproduce since the effective Eddington factors in these methods are always bounded by $\frac{1}{3} \leq f \leq 1$.

Finally, we point out one potential shortcoming of our tests of the RHD algorithms is the paucity of fully dynamical problems. For instance, there is no RHD analogue of a Riemann problem in the test suite, as there were for the HD algorithms (see Paper I) and MHD algorithms (see Paper II). This reflects the difficulty of finding suitable tests for which an analytic solution, or a carefully constructed numerical solution, is already available. Future work with the RHD algorithms in ZEUS-2D will concentrate not only on applications to astrophysical systems, but also on additional tests suitable for the problem of interest. It is our experience that problems involving wave propagation result in the most stringent tests of numerical algorithms, therefore problems involving the propagation of RHD wave modes are excellent candidates for future tests.

We thank Barbara Mihalas for useful discussions, and Randall Bramley for advice regarding sparse matrix solvers. J. S. would like to thank the Department of Astronomy and the National Center for Supercomputing Applications (NCSA) at the University of Illinois for financial support. D. M. expresses thanks to the University of Illinois for providing substantial research funds in support of this project. The computations were performed on the Cray X-MP at the NCSA.

APPENDIX A
SOME FINITE DIFFERENCE FORMULAE

In this Appendix, we give explicit finite difference formula for some of the terms in equations (29) and (30).

1. The $(\nabla \boldsymbol{v} : \mathbf{P}^{n+\theta})_{i,j}$ term:

$$(\nabla \boldsymbol{v} : \mathbf{P}^{n+\theta})_{i,j} = (\nabla \boldsymbol{v}_{(11)})_{i,j} f11_{i,j} E^{n+\theta}_{i,j} + (\nabla \boldsymbol{v}_{(22)})_{i,j} f22_{i,j} E^{n+\theta}_{i,j} + (\nabla \boldsymbol{v}_{(33)})_{i,j}(1 - f11_{i,j} - f22_{i,j}) E^{n+\theta}_{i,j} + \langle (\nabla \boldsymbol{v}_{(12)})_{i,j} \rangle + \langle (\nabla \boldsymbol{v}_{(21)})_{i,j} \rangle \langle P12^{n+\theta}_{i,j} \rangle , \quad (92)$$

where finite difference expressions for $(\nabla \boldsymbol{v}_{(11)})_{i,j}$, $(\nabla \boldsymbol{v}_{(22)})_{i,j}$, and $(\nabla \boldsymbol{v}_{(33)})_{i,j}$ are given in Appendix C in Paper I, and

$$E^{n+\theta}_{i,j} = \theta E^{n+1}_{i,j} + (1 - \theta) E^{n}_{i,j} , \quad (93)$$

$$\langle (\nabla \boldsymbol{v}_{(12)})_{i,j} \rangle = \tfrac{1}{4}[(\nabla \boldsymbol{v}_{(12)})_{i,j} + (\nabla \boldsymbol{v}_{(12)})_{i,j+1} + (\nabla \boldsymbol{v}_{(12)})_{i+1,j} + (\nabla \boldsymbol{v}_{(12)})_{i+1,j+1}] , \quad (94)$$

$$\langle (\nabla \boldsymbol{v}_{(21)})_{i,j} \rangle = \tfrac{1}{4}[(\nabla \boldsymbol{v}_{(21)})_{i,j} + (\nabla \boldsymbol{v}_{(21)})_{i,j+1} + (\nabla \boldsymbol{v}_{(21)})_{i+1,j} + (\nabla \boldsymbol{v}_{(21)})_{i+1,j+1}] , \quad (95)$$

$$(\nabla \boldsymbol{v}_{(12)})_{i,j} = (v2_{i,j} - v2_{i-1,j})/dx1b_i , \quad (96)$$

$$(\nabla \boldsymbol{v}_{(21)})_{i,j} = \frac{(v1_{i,j} - v1_{i,j-1})}{g2a_i dx2b_j} - \frac{(v2_{i,j} + v2_{i-1,j})}{2 g2a_i} \left(\frac{\partial g2a_i}{\partial x_1} \right) , \quad (97)$$

$$\langle P12^{n+\theta}_{i,j} \rangle = \tfrac{1}{4}[P12^{n+\theta}_{i,j} + P12^{n+\theta}_{i+1,j} + P12^{n+\theta}_{i,j+1} + P12^{n+\theta}_{i+1,j+1}] , \quad (98)$$

$$P12^{n+\theta}_{i,j} = f12_{i,j}(E^{n+\theta}_{i,j} + E^{n+\theta}_{i-1,j} + E^{n+\theta}_{i,j-1} + E^{n+\theta}_{i-1,j-1}) . \quad (99)$$

2. The $(\nabla \cdot \boldsymbol{F}^{n+\theta})_{i,j}$ term: we write $\boldsymbol{F}^{n+\theta} = \theta \boldsymbol{F}^{n+1} + (1 - \theta)\boldsymbol{F}^{n}$. From the AFL formula (eq. [26]), which gives an explicit expression for $\boldsymbol{F}^{n+1}$, we can therefore write

$$(\nabla \cdot \boldsymbol{F}^{n+\theta})_{i,j} = \theta(\nabla \cdot \boldsymbol{a}\boldsymbol{F}^{n})_{i,j} + (1 - \theta)(\nabla \cdot \boldsymbol{F}^{n})_{i,j} - \theta\alpha(\nabla \cdot \boldsymbol{b}[\nabla \cdot \boldsymbol{f}E]^{n+1})_{i,j} - \theta(1 - \alpha)(\nabla \cdot \boldsymbol{b}[\nabla \cdot \boldsymbol{f}E]^{n})_{i,j} , \quad (100)$$

where

$$\boldsymbol{a} = (a1, a2) = (\exp[-c\chi^{n+\alpha}_{F1}\Delta t], \exp[-c\chi^{n+\alpha}_{F2}\Delta t]) , \quad (101)$$

$$\boldsymbol{b} = (b1, b2) = \left\{ (1 - \exp[-c\chi^{n+\alpha}_{F1}\Delta t]) \frac{c}{\chi^{n+\alpha}_{F1}} , (1 - \exp[-c\chi^{n+\alpha}_{F2}\Delta t]) \frac{c}{\chi^{n+\alpha}_{F2}} \right\} , \quad (102)$$

$$\chi^{n+\alpha}_{F1} = \alpha\chi^{n+1}_{F1} + (1 - \alpha)\chi^{n}_{F1} , \quad (103)$$

$$\chi^{n+\alpha}_{F2} = \alpha\chi^{n+1}_{F2} + (1 - \alpha)\chi^{n}_{F2} . \quad (104)$$

The $(\nabla \cdot \boldsymbol{a}\boldsymbol{F}^{n})_{i,j}$, $(\nabla \cdot \boldsymbol{F}^{n})_{i,j}$, $(\nabla \cdot \boldsymbol{b}[\nabla \cdot f E]^{n+1})_{i,j}$, and $(\nabla \cdot \boldsymbol{b}[\nabla \cdot f E]^{n})_{i,j}$ terms in equation (100) can all be written as

$$(\nabla \cdot \boldsymbol{q})_{i,j} = \frac{(g2a_{i+1} g31a_{i+1} q1_{i+1,j} - g2a_i g31a_i q1_{i,j})}{dvl1a_i} + \frac{(g32a_{j+1} q2_{i,j+1} - g32a_j q2_{i,j})}{g2b_i dvl2a_j} , \quad (105)$$

where $\boldsymbol{q} = (q1, q2)$ is a vector whose components are centered at the appropriate zone interfaces. Thus, for the $(\nabla \cdot \boldsymbol{a}\boldsymbol{F}^{n})_{i,j}$ term in equation (100), we define the $\boldsymbol{q}$ used in equation (105) as

$$q1_{i,j} = \exp[-c(\chi^{n+\alpha}_{F1})_{i,j}\Delta t] F1^{n}_{i,j} , \quad (106)$$

$$q2_{i,j} = \exp[-c(\chi^{n+\alpha}_{F2})_{i,j}\Delta t] F2^{n}_{i,j} , \quad (107)$$

and $(\chi^{n}_{F1})_{i,j}$ and $(\chi^{n}_{F2})_{i,j}$ [or $(\chi^{n+1}_{F1})_{i,j}$ and $(\chi^{n+1}_{F2})_{i,j}$] are all given functions of $e^{n}_{i,j}$ and $d^{n}_{i,j}$ (or $e^{n+1}_{i,j}$ and $d^{n+1}_{i,j}$) which are evaluated at the appropriate zone faces (see Fig. 1 for centering), for example

$$(\chi^{n}_{F1})_{i,j} = \chi_F(\tfrac{1}{2}[e^{n}_{i-1,j} + e^{n}_{i,j}], \tfrac{1}{2}[d^{n}_{i-1,j} + d^{n}_{i,j}]) , \quad (108)$$

$$(\chi^{n}_{F2})_{i,j} = \chi_F(\tfrac{1}{2}[e^{n}_{i,j-1} + e^{n}_{i,j}], \tfrac{1}{2}[d^{n}_{i,j-1} + d^{n}_{i,j}]) . \quad (109)$$

For the $(\nabla \cdot \boldsymbol{F}^n)_{i,j}$ term in equation (100), we define the $\boldsymbol{q}$ used in equation (105) as

$$q1_{i,j} = F1_{i,j} , \tag{110}$$

$$q2_{i,j} = F2_{i,j} . \tag{111}$$

For the $(\nabla \cdot \boldsymbol{b}[\nabla \cdot fE]^n)_{i,j}$ term in equation (100), we define the $\boldsymbol{q}$ used in equation (105) as

$$q1_{i,j} = b1_{i,j}([\nabla \cdot fE]^n_{(1)})_{i,j} , \tag{112}$$

$$q2_{i,j} = b2_{i,j}([\nabla \cdot fE]^n_{(2)})_{i,j} , \tag{113}$$

where

$$b1_{i,j} = (1 - \exp\,[-c(\chi^{n+\alpha}_{F1})_{i,j}\Delta t])\frac{c}{(\chi^{n+\alpha}_{F1})_{i,j}} , \tag{114}$$

$$b2_{i,j} = (1 - \exp\,[-c(\chi^{n+\alpha}_{F2})_{i,j}\Delta t])\frac{c}{(\chi^{n+\alpha}_{F2})_{i,j}} , \tag{115}$$

$$([\nabla \cdot fE]^n_{(1)})_{i,j} = \frac{(g2b_i^2 g31b_i f11_{i,j}E^n_{i,j} - g2b_{i-1}^2 g31b_{i-1} f11_{i-1,j}E^n_{i-1,j})}{g2a_i dvl1b_i} - \frac{(E^n_{i,j} + E^n_{i-1,j})}{2g2a_i}\left(\frac{\partial g2a_i}{\partial x_1}\right) + \frac{(g32a_{j+1} f12_{i,j+1}\langle E^n_{i,j+1}\rangle - g32a_j f12_{i,j}\langle E^n_{i,j}\rangle)}{g2a_i dvl2a_j} , \tag{116}$$

$$([\nabla \cdot fE]^n_{(2)})_{i,j} = \frac{(g2a_{i+1}^2 g31a_{i+1} f12_{i+1,j}\langle E^n_{i+1,j}\rangle - g2a_i^2 g31a_i f12_{i,j}\langle E^n_{i,j}\rangle)}{g2b_i dvl1a_i} + \frac{(g32b_j^2 f22_{i,j}E^n_{i,j} - g32b_{j-1}^2 f22_{i,j-1}E^n_{i,j-1})}{g2b_i g32a_j dvl2b_j} + \frac{(f11_{i,j}E^n_{i,j} + f11_{i,j-1}E^n_{i,j-1}) - (E^n_{i,j} + E^n_{i,j-1})}{2g2b_i g32a_j}\left(\frac{\partial g32a_j}{\partial x_2}\right) , \tag{117}$$

$$\langle E^n_{i,j}\rangle = \tfrac{1}{4}(E^n_{i,j} + E^n_{i-1,j} + E^n_{i,j-1} + E^n_{i-1,j-1}) . \tag{118}$$

And finally, the expressions for $(\nabla \cdot \boldsymbol{b}[\nabla \cdot fE]^{n+1})_{i,j}$ term in equation (100) are identical to equations (112)–(118) with $E^n_{i,j}$ replaced with $E^{n+1}_{i,j}$.

REFERENCES

Bramley, R. 1989, private communication
Buchler, J. R. 1979, J. Quant. Spectros. Rad. Transf., 22, 293
Castor, J. I. 1972, ApJ, 178, 779
Kaneko, N., Morita, K., & Maekawa, M. 1984, Ap&SS, 107, 333
Klein, R. I., Castor, J., Greenbaum, A., Taylor, D., & Dykema, P. G. 1988, preprint
Kley, W. 1989a, A&A, 208, 98
———. 1989b, A&A, 222, 141
Kunasz, P., & Auer, L. H. 1988, J. Quant. Spectros. Rad. Transf. 39, 67
Lindquist, R. W. 1966, Ann. Phys., 37, 487
Mihalas, B. W. 1988, preprint
Mihalas, D., Auer, L. H., & Mihalas, B. W. 1978, ApJ, 220, 1001
Mihalas, D., & Klein, R. I. 1982, J. Comput. Phy., 46, 97
Mihalas, D., & Mihalas, B. W. 1984, Foundations of Radiation Hydrodynamics (New York: Oxford Univ. Press)
Mihalas, D., & Weaver, R. 1982, J. Quant. Spectros. Rad. Transf., 28, 213
Munier, A., & Weaver, R. 1984, Los Alamos National Laboratory Report LA-UR-84-3872
Richtmyer, R. D., & Morton, K. W. 1957, Difference Methods for Initial-Value Problems, 2d ed. (New York: Wiley)
Stone, J. M., & Mihalas, D. 1991, J. Comput. Phys., in press
Stone, J. M., & Norman, M. L. 1992a, ApJS, 80, 753 (Paper I)
———. 1992b, ApJS, 80, 791 (Paper II)
Winkler, K.-H., & Norman, M. L., eds. 1986, Astrophysical Radiation Hydrodynamics (Dordrecht: Reidel), 71